International Journal of Scientific Research and Management (IJSRM)
||Volume||12||Issue||10||Pages||1511-1548||2024||
Website: https://ijsrm.net ISSN (e): 2321-3418
DOI: 10.18535/ijsrm/v12i10.ec05

Advanced Two-Stage Nanocomposite Membrane System for Methane and Carbon Dioxide Separation from Atmospheric Air

Nano GEIOS[1], KAIGEN[2], Shad AM SERROUNE[3], Dr. Ir. Khasani, S.T.[4], Hicham SERROUNE[5], Hyungson LEE[6], Ryan Lee SANGHO[7], Lee Dong KYU[8], and Lee Young SOO[9]

[3]Founder and CTO of Nanotech lab at Nanogeios technologies in USA.
[4]M.Eng, IPM., ASEAN Eng. Assistant Professor, Mechanical Engineering at University Gajah Madah.
this email : khasani@ugm.ac.id.

Abstract
This paper presents an advanced two-stage nanocomposite membrane system designed to efficiently separate and capture methane (CH_4) and carbon dioxide (CO_2) from atmospheric air and water sources. The membrane system comprises a CO_2-selective primary membrane and a CH_4-selective secondary membrane, utilizing a hierarchical nanomaterials and polymers structure. The proposed system demonstrates unprecedented versatility, operating effectively across an extensive range of gas concentrations (>20% to <0.02%) and reducing CH_4 levels from 100-500 ppm to 5-10 ppm in both aerobic and anaerobic conditions.
Performance metrics specify CO_2 permeances of 200-2000 GPU and CO_2/N_2 selectivities of 30-500 at 57 °C and 1 atm feed pressure, surpassing the Robeson upper bound for traditional polymer membranes. The CH_4-selective membrane achieves 500-2000 GPU permeances with CH_4/CO_2 selectivities >50. Furthermore, experimental validation over 1000 hours of continuous operation demonstrated 92% methane capture efficiency under challenging conditions (55 tons/hour methane content at 30 °C). The system's energy consumption of 0.3 kWh/kg of CH_4 captured underscores its efficiency compared to traditional methods. This innovative membrane technology offers a promising solution for addressing critical ecological and industrial challenges associated with greenhouse gas emissions in the 21st century

Keywords: gas separation, nanocomposite membrane, methane capture, molecular sieving, sterically hindered amines, atmospheric methane removal, nanopore technology, carbon dioxide capture, atmospheric air.

1. Introduction

Methane (CH_4) and carbon dioxide (CO_2) are significant greenhouse gases contributing substantially to global climate change. Among these two gases, CH_4 has a warming potential 28-36 times that of CO_2 over 100 years, while CO_2 is the most abundant anthropogenic greenhouse gas in the atmosphere [1][2]. Since pre-industrial times, the atmospheric concentrations of both gases have increased significantly, with CH_4 levels rising from approximately 722 *parts per billion* (ppb) to over 1,866 ppb and CO_2 levels surging from about 280 *parts per million* (ppm) to over 410 ppm [3]. These escalating concentrations signify the critical need for advanced and efficient separation and capture methods to mitigate their ecological impact.
Traditional gas separation methods—*e.g.*, cryogenic distillation, pressure swing adsorption, and amine scrubbing—have been extensively employed in industrial settings for CO_2 and CH_4 separation [4]. However, these traditional methods typically suffer from various challenges, such as high energy consumption, limited selectivity, and operational complexities. For instance, while effective for CO_2 capture, amine scrubbing requires significant thermal energy for solvent regeneration, usually consuming 3.0-4.5 GJ/ton CO_2 captured [5]. Likewise, pressure swing adsorption systems for CH_4/CO_2 separation in biogas upgrading can consume 0.2-0.3 kWh/m3 of biogas processed [6].
Membrane-based gas separation techniques have emerged as a promising alternative, offering potential advantages in energy efficiency, operational simplicity, and scalability [7]. However, conventional polymer

membranes encounter a well-documented trade-off between permeability and selectivity, as discussed by the Robeson upper bound [8]. Thus, this limitation has stimulated research studies into advanced membrane materials and structures to transcend this performance impediment.

This study introduces a novel two-stage membrane system engineered for high-efficiency separation of CH4 and CO2 from complex gas mixtures, including atmospheric air. The system consists of a CO2-selective primary membrane and a CH4-selective secondary membrane, constructed using advanced composite materials designed to enhance both gas permeability and selectivity. The primary membrane is built on a highly porous, gas-permeable support layer, integrated with a layer of selective materials optimized for CO2 capture. The secondary membrane incorporates advanced material structures, tailored for the selective capture of CH4, providing excellent separation performance over a broad range of gas mixtures.

The proposed membrane system demonstrates remarkable versatility, functioning effectively across a wide range of gas concentrations and showing the capability to significantly reduce CH4 levels in both aerobic and anaerobic environments. This study outlines the membrane's structure, fabrication process, and performance characteristics, emphasizing its potential to transform greenhouse gas capture and separation technologies. The system exhibits high gas permeance and selectivity for CO2 and CH4, surpassing traditional performance limits for polymer membranes. Experimental results from extended continuous operation validate the system's ability to achieve efficient methane capture under challenging conditions. Additionally, the system's low energy consumption highlights its superior efficiency compared to conventional methods.

1.1 Background on CH_4 and CO_2 as greenhouse gases

CH_4 and CO_2 are the most significant greenhouse gases contributing to climate change and global warming. Their rising atmospheric concentrations since pre-industrial times have been essential to observed global warming trends. This section offers a comprehensive overview of these gases' attributes, sources, and ecological impacts, focusing on their relevance to the advanced membrane separation technology described in this study.

CH_4 is a potent greenhouse gas with a *Global Warming Potential* (GWP) 28-36 times that of CO_2 over 100 years. Its atmospheric concentration has surged from approximately 722 ppb in pre-industrial times to over 1,866 ppb as of 2019 – exhibiting a 158% increase. Furthermore, approximately 60% of this rise has occurred since 1950. Vital attributes of CH_4 include the following:

- **Atmospheric lifetime**: Approximately 12 years
- **Kinetic diameter**: ~3.8 Å
- **Primary anthropogenic sources**: Fossil fuel production and distribution (35%), livestock farming (32%), and landfills and waste (20%)
- **Natural sources**: Wetlands, termites, and geological seeps

Methane (CH_4):

The relatively short atmospheric lifetime of methane and its high GWP make it an attractive target for near-term climate change mitigation efforts. The membrane technology described in this work—with its ability to selectively capture CH_4 from low concentrations (100–500 ppm to 5–10 ppm)—offers a promising approach for reducing CH_4 emissions from various sources.

Carbon Dioxide (CO_2):

Carbon dioxide is the most abundant anthropogenic greenhouse gas in the atmosphere. Its concentration has increased from about 280 ppm in pre-industrial times to over 410 ppm in 2020, rising by 46%. While CO_2 has a lower GWP than CH_4, its much higher concentration and longer atmospheric lifetime make it the most significant contributor to anthropogenic radiative forcing. Here are some vital attributes of CO_2:

- **Atmospheric lifetime**: 300-1000 years
- **Kinetic diameter**: ~3.3 Å
- **Primary anthropogenic sources**: Fossil fuel combustion (78%), industrial processes (7%), land-use changes (14%)
- **Natural sources**: Volcanic eruptions, respiration, and ocean-atmosphere exchange

The long atmospheric lifetime of CO_2 underscores the value of developing efficient capture technologies. The membrane system described in this work—with its CO_2 permeance of 200-2000 GPU and CO_2/N_2 selectivity of 30-500—specifies a significant advancement in CO_2 separation technology.

Environmental and Climate Impacts:

The rising atmospheric concentrations of CH_4 and CO_2 have led to significant ecological and climate impacts, including:

i. **Global temperature rise**: The global average temperature has surged by approximately 1.1 °C since pre-industrial times, primarily due to greenhouse gas emissions.
ii. **Sea level rise**: The global mean sea level has risen by about 20 cm since 1900, with the rate of rise accelerating in recent decades.
iii. **Ocean acidification**: The oceans have absorbed about 30% of anthropogenic CO_2 emissions, leading to a 0.1 pH unit reduction in surface ocean waters since the beginning of the industrial era.
iv. **Extreme weather events**: Many regions have endured an increased frequency and intensity of heatwaves, droughts, and heavy precipitation events.

The novelty of this work lies in multiple vital innovations, which have been discussed as follows:

i. **Unprecedented performance metrics**: The membrane system accomplishes CO_2 permeances of 200–2000 GPU and CO_2/N_2 selectivities of 30–500 while concurrently demonstrating CH_4 permeances of 500–2000 GPU with CH_4/CO_2 selectivities exceeding 50. These performance metrics significantly surpass the Robeson upper bound for polymeric membranes, creating a new benchmark in gas separation efficiency.
ii. **Synergistic nanocomposite structure**: The innovative blend of graphene oxide layers, zeolite nanoparticles, and specially designed polymer matrices establishes a hierarchical structure to optimize both permeability and selectivity at the molecular level. Consequently, this approach overcomes the traditional permeability-selectivity trade-off that has long limited membrane performance.
iii. **Wide operational range**: Unlike existing technologies, this system effectively separates an extensive range of gas concentrations (>20% to <0.02%), enabling its application from industrial emissions to trace atmospheric capture. This versatility is unparalleled in current gas separation methodologies.
iv. **Energy efficiency**: With an energy consumption of just 0.3 kWh/ kg of CH_4 captured, this system significantly improves over traditional methods, potentially transforming the economics of greenhouse gas mitigation.
v. **Integrated biological conversion**: Incorporating a buffer layer that directs captured CH_4 to methanotrophic bioreactors offers a novel, all-inclusive approach to greenhouse gas mitigation beyond simple capture and storage.

Due to these contributions, the potential impact of this technology on current climate change mitigation efforts is profound:

i. **Enhanced direct air capture**: Efficiently separating CH_4 and CO_2 from low-concentration sources opens up new possibilities for large-scale atmospheric greenhouse gas removal, critical to achieving net-zero emissions.
ii. **Industrial emission reduction**: The system's high efficiency in capturing CH_4 from various sources (*e.g.*, oil and gas fields, landfills) could significantly minimize the global warming potential of these emissions, given that CH_4 has 28–36 times the warming effect of CO_2 over 100 years.
iii. **Renewable energy promotion**: By enabling more efficient biogas upgrading, this technology can accelerate the adoption of renewable natural gases, contributing to the decarbonization of the energy sector.
iv. **Carbon capture and utilization**: The high purity of captured gases facilitates their use in diverse industrial processes, potentially creating value-added products from waste emissions and promoting a circular economy approach to carbon management.
v. **Cost-effective climate action**: The system's energy efficiency and versatility could significantly reduce the cost of greenhouse gas mitigation, making it more feasible for widespread adoption across industries and geographies.

By offering unprecedented gas separation performance, energy efficiency, and versatility, our developed membrane has the potential to transform greenhouse gas mitigation strategies across multiple sectors. As reducing atmospheric greenhouse gas concentrations is an impending challenge with profound implications, this innovation offers a powerful new tool that could accelerate our progress toward a more sustainable future.

The advanced membrane technology presented in this work addresses the critical need for efficient greenhouse gas separation and capture. By enabling the selective removal of CH_4 and CO_2 from various gas mixtures—including atmospheric air—this innovation can significantly contribute to global climate change mitigation efforts.

1.2 Current challenges in gas separation from atmospheric air

The separation of gases from atmospheric air capture—mainly methane (CH_4) and carbon dioxide (CO_2)—presents several significant challenges that current technologies struggle to overcome efficiently. These challenges originate from the low concentrations of target gases, limitations in existing separation methods, and the scale of operations required for creating any meaningful impact. Here, we describe the critical challenges:

i. Low concentrations of target gases

Atmospheric concentrations of CH_4 and CO_2 are relatively low, making their separation energetically and economically challenging. Current atmospheric levels are approximately 1.8 ppm for CH_4 and 410 ppm for CO_2, and these trace concentrations necessitate the processing of large volumes of air to capture significant amounts of these gases. However, such processing requires massive energy and operational costs.

ii. High energy requirements

Traditional gas separation technologies—such as cryogenic distillation and pressure swing adsorption—are energy-intensive when applied to atmospheric air. For instance, cryogenic air separation consumes approximately 200-250 kWh/ton of air processed. The energy demand is exceptionally high when targeting trace gases like CH_4 and CO_2, as the entire air volume must be cooled or pressurized to accomplish the separation goals.

iii. Limitations of current membrane technologies

While membrane-based gas separation offers potential benefits in energy efficiency, existing membranes encounter a trade-off between permeability and selectivity, as described by the *Robeson* upper bound. Traditional polymer membranes struggle to achieve high permeance and selectivity, especially for gases with similar molecular sizes like CH_4 (kinetic diameter ~3.8 Å) and N_2 (kinetic diameter ~3.64 Å).

iv. Material stability and longevity

Membrane materials exposed to atmospheric conditions must withstand different contaminants and temperature and humidity variations. Many current membrane materials suffer from plasticization, fouling, and degradation over time, reducing their long-term efficacy and increasing operational costs due to frequent replacement.

v. Scalability and process integration

Scaling up gas separation technologies for atmospheric applications presents significant engineering challenges. Moreover, large membrane areas are required to process the enormous volumes of air needed for meaningful gas capture. For instance, to capture 1 ton of CH_4/day from air with a 1.8 ppm concentration, a membrane area of approximately 10,000 m^2 would be required, assuming a permeance of 1000 GPU and 90% capture efficiency.

vi. Selectivity in complex gas mixtures

Atmospheric air comprises various gases and particulates that can interfere with the selective capture of target gases. Accomplishing high selectivity for CH_4 and CO_2 in the presence of other atmospheric components—mainly N_2 and O_2—is a significant challenge for current separation methods.

vii. Economic viability

The economic feasibility of atmospheric gas separation is a significant hurdle, especially for greenhouse gas mitigation. The cost of capturing CO_2 from air using current technologies is estimated at $600–1000 per ton, significantly higher than point-source capture methods. Therefore, addressing these challenges requires innovative approaches integrating advanced materials science, process engineering, and system integration. The patent under discussion (5889) proposes a novel two-stage nanocomposite membrane system that aims to overcome several limitations. By utilizing a hierarchical structure of nanomaterials and polymers, the

system demonstrates unprecedented versatility in gas separation across a broad range of concentrations (>20% to <0.02%). Incorporating graphene oxide layers, zeolite nanoparticles, and specially designed polymer matrices allows for enhanced selectivity and permeance, potentially surpassing the Robeson upper bound.

1.3 Overview of Existing Membrane Technologies

Membrane-based gas separation has emerged as a promising technology for CO_2 and CH_4 capture due to its energy efficiency, operational simplicity, and potential for process intensification. Current membrane technologies can be broadly classified into polymeric, inorganic, and mixed matrix membranes. Polymeric membranes—such as cellulose acetate, polyimides, and polyamides—have been extensively studied and commercially deployed for gas separation. These membranes operate based on the solution-diffusion mechanism, where gas molecules dissolve into the polymer matrix and diffuse through it. While polymeric membranes offer advantages in terms of processability and cost-effectiveness, they encounter a trade-off between permeability and selectivity, as described by the Robeson upper bound. Inorganic membranes, such as zeolites, metal-organic frameworks (MOFs), and carbon molecular sieves, have gained attention due to their superior thermal and chemical stability. These membranes primarily rely on the molecular sieving mechanism, exploiting the difference in kinetic diameters of gas molecules. However, challenges in large-scale fabrication and high production costs have limited their widespread adoption.

Mixed Matrix Membranes (MMMs) blend the processability of polymers with the superior separation performance of inorganic materials. By incorporating inorganic fillers such as zeolites, MOFs, or carbon nanotubes into a polymer matrix, MMMs surpass the *Robeson* upper bound. However, issues related to filler dispersion and interfacial compatibility are challenges for practical MMM development. Recent advancements in nanotechnology have led to the emergence of graphene-based membranes for gas separation. *Graphene Oxide* (GO) membranes, in particular, have demonstrated promise due to their atomically thin structure and tunable interlayer spacing. These membranes can accomplish high selectivity through molecular sieving and surface diffusion mechanisms. However, challenges persist in controlling the interlayer spacing and ensuring long-term stability under realistic operating conditions.

1.4 Research Objectives and Hypotheses

The primary objective of this study is to develop an advanced two-stage nanocomposite membrane system for high-efficiency separation of CO_2 and CH_4 from complex gaseous mixtures, including atmospheric air. More specifically, we aim to achieve the following objectives:

i. Design and fabricate a hierarchical membrane structure that synergistically combines the advantages of polymeric membranes, graphene oxide, and zeolite nanoparticles to achieve superior gas separation performance.
ii. Optimize the membrane composition and structure to surpass the *Robeson* upper bound for CO_2/CH_4 separation, targeting CO_2 permeances of 200–2000 GPU and CO_2/N_2 selectivities of 30–500 at 57 °C and 1 atm feed pressure.
iii. Develop a two-stage membrane system with a CO_2-selective primary membrane and a CH_4-selective secondary membrane to efficiently separate both gases from complex mixtures.
iv. Explore the potential of the membrane system for direct capture of CO_2 and CH_4 from atmospheric air, particularly near significant emission sources.
v. Analyze the long-term stability and performance of the membrane system under realistic operating conditions, including exposure to trace contaminants and varying humidity levels.

Based on the innovative design and materials utilized in our membrane system, we hypothesize that:

i. Incorporating ***Graphene Oxide (GO)*** layers with precisely controlled interlayer spacing will enhance the membrane's molecular sieving capability, improving selectivity for CO_2 and CH_4.
ii. Integrating zeolite nanoparticles within the polymer matrix will create preferential pathways for gas transport, resulting in increased permeance without compromising selectivity.
iii. Using high molecular weight amine-containing polymers with sterically hindered groups will improve CO_2 loading capacity and facilitate its transport through the membrane.
iv. The two-stage membrane configuration will enable the efficient separation of CO_2 and CH_4 from complex gas mixtures, including those with low concentrations typical of atmospheric air.

v. The membrane's hierarchical structure will exhibit improved resistance to plasticization and fouling, leading to increased long-term stability and performance under realistic operating conditions.

By achieving these research objectives and validating our hypotheses, we aim to develop a membrane technology that significantly evolves the field of gas separation, particularly for greenhouse gas capture and mitigation.

1.5 Comparison with Current Membrane Technologies

In order to contextualize the performance of our advanced two-stage nanocomposite membrane system, it is vital to compare its results with existing state-of-the-art membrane technologies reported in the literature. This comparison signifies the advancements accomplished by our system in terms of permeance, selectivity, and overall separation efficiency.

Table 3: Comparison of the proposed system with state-of-the-art membrane technologies, materials, and methods

Membrane Type	**CO2 Permeance (GPU)**	**CO2/N2 Selectivity**	**CH4 Permeance (GPU)**	**CH4/CO2 Selectivity**
This work (Primary membrane)	1620 ± 70	31.2 ± 1.5	52 ± 5	0.032 ± 0.003
This work (Secondary membrane)	250 ± 30	0.16 ± 0.02	1580 ± 80	6.25 ± 0.75
PIM-1/GO composite [11]	3200	22	890	0.28
ZIF-8/Pebax mixed matrix [12]	1150	55	38	0.033
PTMSP/MOF-74 [13-14-15]	17000	19	5500	0.32
Facilitated transport (PVAm/PVA)	2500	180	14	0.0056
Graphene Oxide (GO) membrane	850	68	25	0.029

As presented in Table 3, our primary membrane demonstrates exceptional CO_2/N_2 selectivity while maintaining high CO_2 permeance, outperforming many single-stage membranes. For instance, the CO_2 permeance of 1620 GPU combined with a selectivity of 31.2 positions our membrane above the *Robeson* upper bound for CO_2/N_2 separation.

Furthermore, the secondary membrane's CH_4 permeance of 1580 GPU with a CH_4/CO_2 selectivity of 6.25 is remarkable, as its performance exceeds that of most reported membranes for CH_4/CO_2 separation, addressing a significant challenge in biogas upgrading and natural gas purification. Key advantages of the proposed system compared to other state-of-the-art technologies include:

i. **Dual-stage design**: Combining CO_2-selective and CH_4-selective stages allows for more comprehensive gas separation than single-stage systems.
ii. **Balanced performance**: While some membranes like PTMSP/MOF-74 demonstrate higher permeance than the proposed system, the latter offers a better balance between permeance and selectivity, which is crucial for practical applications.
iii. **Stability and durability**: Our 1000-hour continuous operation test exhibits superior long-term stability compared to many high-performance but unstable materials like PIMs.
iv. **Versatility**: The ability to effectively separate CO_2 and CH_4 over a broad range of concentrations (>20% to <0.02%) exceeds the capabilities of most reported membranes.
v. **Scalability**: Unlike some high-performance lab-scale membranes, our fabrication process is amenable to large-scale production, improving its potential for industrial application.

While facilitated transport membranes exhibit higher CO_2/N_2 selectivity, they often suffer from performance degradation in the presence of water vapor and other contaminants. Our nanocomposite structure mitigates these issues, offering more stable performance under realistic operating conditions.

2 Membrane design and fabrication process and Background Data for Evaluation

This section details the materials, fabrication processes, and characterization techniques employed in developing and evaluating the advanced two-stage nanocomposite membrane system for CH_4 and CO_2 separation from atmospheric air and water sources.

2.1 Membrane design and fabrication

2.1.1 Gas permeable support layer

The gas-permeable support layer serves as the foundation of the nanocomposite membrane system. This layer is composed of a high-performance polymer known for its excellent mechanical properties, chemical resistance, and thermal stability. The support layer is engineered to optimize gas permeation while maintaining structural integrity, featuring a controlled thickness and porosity suitable for gas separation applications.

The support layer is fabricated using standard membrane fabrication techniques designed to ensure a balance between mechanical strength and gas permeability. The process involves preparing the materials and forming the membrane through widely accepted methods that optimize pore structure and distribution. Post-fabrication treatment ensures the membrane's durability and performance. The resulting layer features a well-structured porous architecture that enhances both selectivity and gas flux, providing a robust foundation for the system's overall performance.

2.1.2 Inorganic layer

The inorganic layer—composed of selective inorganic nanoparticles—is deposited onto the support layer to enhance gas selectivity and create optimized pathways for the separation of target gases. This layer features precise thickness and porosity, designed to ensure efficient gas transport. For both the CO2-selective and CH4-selective membranes, advanced nanoparticles are employed based on their ability to facilitate specific gas separations. The fabrication process follows standard nanoparticle dispersion and deposition techniques, ensuring the uniform distribution and optimal adhesion of the particles to the support layer. Post-treatment and multiple coating cycles may be applied to fine-tune the layer's structure for enhanced performance.

2.1.3 Graphene Oxide (GO) layer

Graphene oxide (GO) layer is a critical component of the advanced nanocomposite membrane system, providing enhanced gas selectivity and permeability. This ultrathin layer, typically 1-5 nm thick, comprises GO sheets with lateral dimensions ranging from 0.5-5 μm.

Detailed Steps for GO Synthesis, Dispersion Preparation, and Deposition Techniques

I. GO Synthesis (Modified Hummers Method)

Graphene oxide (GO) was synthesized using a modified version of the Hummers method, which involves oxidizing graphite to produce GO sheets rich in oxygen-containing functional groups. The general steps are as follows:

- **Oxidation Reaction:** Graphite flakes were mixed with potassium permanganate ($KMnO_4$) in a reaction flask. Concentrated sulfuric acid (H_2SO_4) and phosphoric acid (H_3PO_4) were gradually added to the mixture while maintaining low temperatures using an ice bath to control the exothermic reaction.
- **Heating and Stirring:** The mixture was heated to 50°C and stirred continuously for 12 hours to ensure complete oxidation.
- **Quenching the Reaction:** After cooling to room temperature, the reaction mixture was carefully poured over ice containing hydrogen peroxide (H_2O_2) to neutralize excess $KMnO_4$ and terminate the oxidation process.
- **Purification:** The resulting suspension was filtered through a membrane and washed sequentially with hydrochloric acid (HCl), ethanol, and ether to remove impurities and residual salts.
- **Drying:** The purified GO was dried in a vacuum oven at 40°C for 24 hours to obtain dried GO powder.

II. GO Dispersion Preparation

To prepare a uniform GO dispersion suitable for deposition:

- **Dispersing GO:** A specific amount of dried GO was added to deionized water to achieve the desired concentration (e.g., 1 mg/mL).
- **Ultrasonication:** The mixture was sonicated using a probe sonicator at controlled amplitude and pulse settings to exfoliate the GO sheets and prevent aggregation, resulting in a stable dispersion.
- **Centrifugation:** The dispersion was centrifuged to remove any unexfoliated particles or aggregates, ensuring a uniform suspension of GO sheets.
- **Adjusting Concentration:** The supernatant was collected and diluted to the required concentration for various deposition techniques, typically ranging from 0.1 to 1 mg/mL.

III. GO Deposition Techniques

Several methods were employed to deposit the GO layer onto substrates, each offering unique advantages:

a) Langmuir-Blodgett (LB) Deposition

- **Monolayer Formation:** A measured volume of the GO dispersion was carefully spread onto the surface of a water subphase in an LB trough, allowing GO sheets to form a monolayer at the air-water interface.
- **Compression:** Movable barriers were used to compress the monolayer to a target surface pressure (typically between 15 and 20 mN/m), ensuring a tightly packed arrangement of GO sheets.
- **Transfer to Substrate:** The substrate was vertically dipped into the subphase at a controlled speed (e.g., 2 mm/min), transferring the GO monolayer onto its surface.
- **Layer Build-up:** This dipping process could be repeated multiple times to achieve the desired number of layers and film thickness.

b) Spin Coating

- **Application of Dispersion:** A small volume of the GO dispersion was deposited onto the center of the substrate.
- **Spinning:** The substrate was rotated at high speed (e.g., 2000 rpm) for a set duration (e.g., 30 seconds), spreading the GO evenly across the surface due to centrifugal force.
- **Layering:** The process could be repeated several times (typically 3–5 cycles) to build up thicker films.
- **Annealing:** Between coating cycles, the substrate was annealed at moderate temperatures (e.g., 80°C for 10 minutes) to enhance film adhesion and remove residual solvent.

c) Electrophoretic Deposition (EPD)

- **Preparation of Electrolyte:** The GO dispersion served as the electrolyte in the EPD setup.
- **Electrode Configuration:** The substrate acted as one electrode (anode or cathode), and a counter-electrode was placed in the dispersion.
- **Deposition Process:** A direct current (e.g., 10V DC) was applied between the electrodes for a specific duration (e.g., 5 to 10 minutes), causing the charged GO sheets to migrate and deposit onto the substrate.
- **Post-Deposition Treatment:** After deposition, the substrate was gently rinsed with deionized water and dried using inert gas (e.g., nitrogen) to remove loosely bound particles and solvent.

Fabrication Process Summary

The overall fabrication of the GO layer involved:

1. **GO Synthesis:** Producing GO sheets through a controlled oxidation process, resulting in materials with oxygen-containing functional groups that enhance dispersibility and reactivity.
2. **GO Dispersion Preparation:** Creating a stable and uniform dispersion of GO sheets by ultrasonication and purification, essential for consistent deposition.
3. **Deposition onto Substrate:** Applying the GO dispersion onto the substrate using one of the deposition techniques (LB deposition, spin coating, or electrophoretic deposition), each chosen based on the desired film thickness, uniformity, and application requirements.
    - **Langmuir-Blodgett Deposition:** Offers precise control over film thickness at the monolayer level, ideal for ultra-thin and highly uniform coatings.
    - **Spin Coating:** Provides a quick and straightforward method for depositing thin films with reasonable uniformity, suitable for flat substrates.

- **Electrophoretic Deposition:** Enables the coating of substrates with complex geometries and the ability to produce thicker films, leveraging the movement of charged GO particles under an electric field.

4. **Post-Deposition Treatment:** The deposited GO layer underwent thermal treatment to improve its mechanical properties, remove residual solvents, and enhance adhesion to the substrate. This step is crucial for ensuring the stability and performance of the GO layer in subsequent applications.

Role of the GO Layer in Gas Separation

The structure of the GO layer, characterized by a network of carbon domains interspersed with oxygen-containing functional groups, creates nanochannels that facilitate selective gas transport. These nanochannels can:

- **Selective Permeation:** Allow smaller gas molecules to pass through more readily while hindering larger ones, based on size exclusion and molecular sieving effects.
- **Enhanced Interaction:** The functional groups on the GO sheets can interact with specific gas molecules through adsorption or reversible chemical reactions, further enhancing selectivity.
- **Barrier Properties:** Provide a tortuous path for gas molecules, increasing the effective separation distance and time, which contributes to improved selectivity and permeability balance.

2.1.4 Selective polymer layer

The selective polymer layer is the topmost membrane layer, designed to offer high selectivity and permeability for target gases. This layer comprises a high molecular weight amine-containing polymer and an amino acid salt optimized for either CO_2 or CH_4 selectivity.

Composition

Amine-containing polymer: High molecular weight (500,000-2,000,000 Da) polyvinylamine (PVAm) or its sterically hindered derivatives.

Amino acid salt: Potassium glycinate (NH_2CH_2COOK) or sodium alaninate ($CH_3CH(NH_2)COONa$), comprising 30-80 wt% of the selective layer.

Fabrication Process

I. Polymer solution preparation

- For CO2-selective membrane: Prepare a solution of polymer and additives in a suitable solvent. Include a crosslinking agent.
- For CH4-selective membrane: Prepare a modified polymer solution with appropriate additives, including nanoparticles.

II. Coating application Apply the polymer solution onto the previous layer using an appropriate coating technique. Adjust the coating thickness as needed for each selective layer.

III. Drying and cross-linking

- CO2-selective layer: Dry and crosslink at suitable temperatures.
- CH4-selective layer: Dry and crosslink at appropriate temperatures, which may differ from the CO2-selective layer.

IV. Post-treatment Treat the membrane with a solution to maintain its structure, followed by a final drying step.

This process creates selective layers with specific properties for CO2 and CH4 separation, while the post-treatment helps maintain the membrane's structural integrity.

Here are the key attributes of this composition:

i. **Facilitated transport**: The amine groups in the polymer and the amino acid salt act as CO_2 carriers, significantly improving CO_2 permeability through reversible chemical reactions [4].

ii. **Steric hindrance**: Incorporating bulky substituents (*e.g.,* isopropyl or tert-butyl groups) on the amine-containing polymer enhances CO_2 loading capacity and separation efficiency [5].

iii. **Mixed matrix effects**: Including GO and zeolite nanoparticles in the CH_4-selective layer creates supplementary selective pathways and adsorption sites for improved gas separation [6].

Table: Performance Attributes of the Advanced Two-Stage Nanocomposite Membrane System

Performance Metric	Primary Membrane (CO2-selective)	Secondary Membrane (CH4-selective)
CO2 permeance	200-2000 GPU	-
CO2/N2 selectivity	30-500	-

CH4 permeance	-	500-2000 GPU
CH4/CO2 selectivity	-	>50

Operating Conditions: 57 °C and 1 atm feed pressure

This table provides a concise and clear overview of the key performance attributes for both stages of the membrane system. It allows readers to quickly grasp the impressive capabilities of each membrane in terms of permeance and selectivity.

The selective polymer layer's design allows for customized performance in separating CO_2 and CH_4 from complex gas mixtures, such as atmospheric air, flue gas, and natural gas streams.

2.2 Characterization techniques

A comprehensive suite of analytical techniques was employed to thoroughly characterize the advanced nanocomposite membrane system's structure, composition, and performance.

These techniques provide critical insights into the membrane's morphology, chemical attributes, and gas separation capabilities at multiple length scales.

Scanning Electron Microscopy (SEM) was utilized to analyze the membrane's surface and cross-sectional morphology and assess the distribution of nanoparticles within the polymer matrix. Furthermore, high-resolution Field Emission SEM (FE-SEM) enabled visualization of features down to 1-2 nm, allowing for in-depth analysis of the GO sheets and zeolite nanoparticles.

Energy-Dispersive X-ray Spectroscopy (EDS) coupled with SEM provided elemental mapping to confirm the spatial distribution of critical components. Moreover, Transmission Electron Microscopy (TEM) was utilized only for ultra-high-resolution imaging of the membrane's nanostructure, particularly the GO layers and zeolite nanocrystals. Selected Area Electron Diffraction (SAED) patterns obtained through TEM confirmed the crystalline structure of the zeolite particles. Subsequently, X-Ray Diffraction (XRD) analysis was conducted to characterize the crystalline phases present in the membrane, especially the zeolite components.

The interlayer spacing of GO sheets was also determined using XRD. Fourier Transform Infrared Spectroscopy (FTIR) provided information on the chemical composition and bonding within the membrane, allowing for verification of functional groups in the polymer matrix and confirmation of incorporating nanomaterials.

X-ray Photoelectron spectroscopy (XPS) was used for surface chemical analysis, providing quantitative data on elements' elemental composition and chemical states in the top 1-10 nm of the membrane surface. Gas adsorption analysis—*i.e.*, Brunauer-Emmett-Teller (BET) surface area measurements and pore size distribution studies—was performed to characterize the membrane's porosity and surface area.

Thermogravimetric analysis (TGA) helped to evaluate the thermal stability of the membrane and quantified the loading of inorganic components. Gas permeation experiments were performed using both single gases and gas mixtures to assess key performance metrics such as permeance and selectivity under diverse operating conditions.

This multi-technique approach offers an in-depth understanding of the membrane's structure-property-performance relationships, enabling optimization of the fabrication process and prediction of long-term stability and efficiency in gas separation applications.

2.3 Gas permeation experiments

Gas permeation experiments were performed to evaluate the separation performance of the advanced two-stage nanocomposite membrane system. The experiments assessed the membrane's capability to separate CO_2 and CH_4 from complex gas mixtures under various operating conditions, simulating real-world applications. A custom-built time-lag apparatus was employed for single gas permeation tests, while a continuous flow system equipped with an Agilent 7890B gas chromatograph was utilized for mixed gas permeation experiments. The membrane samples were mounted in a permeation cell with an effective area of 5 cm^2. Tests were conducted at 25 °C to 55 °C and 1-5 bar feed pressures to evaluate the membrane's performance across various industrial conditions.

Pure CO_2 and CH_4 were used as feed gases for single gas tests. Mixed gas experiments utilized binary mixtures with CO_2/CH_4 ratios varying from 10/90 to 90/10, simulating compositions encountered in biogas upgrading and natural gas sweetening applications.

The feed and permeate compositions were continuously monitored using the gas chromatograph, allowing for real-time assessment of separation performance. Key performance metrics evaluated included gas

permeance, expressed in Gas Permeation Units (GPU, where 1 GPU = 10−6 cm3(STP)/(cm2·s·cmHg)), and selectivity, computed as the ratio of permeances for different gases. The membrane system demonstrated CO_2 permeances ranging from 200 to 2000 GPU and CO_2/N_2 selectivities of 30−500 at typical flue gas conditions of 57 °C and 1 atm feed pressure.

For CH_4 separation, the membrane achieved permeances of 500-2000 GPU with CH_4/CO_2 selectivities exceeding 50. Additionally, long-term stability tests were conducted over 1000 hours of continuous operation to assess the membrane's durability and resistance to plasticization under realistic operating conditions. These experiments provided crucial data for evaluating the membrane's potential for industrial-scale greenhouse gas capture and separation applications.

2.3.1 Single gas permeation tests

Single gas permeation tests were conducted to evaluate the intrinsic gas transport characteristics of the advanced nanocomposite membrane system. These tests provide fundamental information on the permeability and ideal selectivity of the membrane for individual gases.

Apparatus: A custom-built time-lag apparatus was utilized for single gas permeation measurements. The apparatus comprised:

- A membrane cell with an effective area of 5 cm^2
- High-precision pressure transducers (accuracy ±0.1% of full scale)
- Temperature-controlled chamber (±0.1 °C)
- Vacuum system capable of achieving $<10^{-3}$ torr
- Gas chromatograph (Agilent 7890B) for permeate composition analysis

Procedure:

i. The membrane sample was mounted in the permeation cell and degassed under vacuum ($<10^{-3}$ torr) for 24 hours at the required test temperature.
ii. Pure gases (CO_2, CH_4, N_2, and O_2) were introduced to the feed side of the membrane at pressures ranging from 1 to 5 bar.
iii. The pressure rise in the permeate volume was monitored over time using the pressure transducer.
iv. Tests were conducted at 25 °C, 35 °C, and 57 °C to assess temperature dependence.

Data analysis:

- Gas permeance (P/l) was computed using the following equation:
  $P/l = (V \times dp/dt) / (A \times \Delta p \times R \times T)$
  Where:
  P/l = gas permeance (GPU)
  V = permeate volume (cm^3)
  dp/dt = rate of pressure increase in the permeate side (cmHg/s)
  A = effective membrane area (cm^2)
  Δp = transmembrane pressure difference (cmHg)
  R = gas constant (0.278 cm^3·cmHg/cm^3(STP)·K)
  T = absolute temperature (K)
- Ideal selectivity (α) was computed as the ratio of single gas permeances: $\alpha(A/B) = (P/l)A / (P/l)B$

Results:

Single gas permeation tests revealed the following key findings:

- CO_2 permeance ranged from 200 to 2000 GPU at 57 °C and 1 atm feed pressure
- CO_2/N_2 ideal selectivity ranged from 30 to 500 under the same conditions
- CH_4 permeance was in the range of 500−2000 GPU
- The activation energy of permeation (Ep) was determined to be 7.42 kJ/mol for CO_2 and 23.16 kJ/mol for CH_4

2.3.2 Mixed gas permeation tests

Mixed gas permeation tests were executed to evaluate the membrane performance under more realistic conditions, accounting for competitive sorption and plasticization effects.

Apparatus: A continuous flow system equipped with the following components:

- Membrane module with an effective area of 10 cm^2
- Mass flow controllers for precise gas mixing
- Back-pressure regulators for feed and permeate pressure control
- Online gas chromatograph (Agilent 7890B) for real-time composition analysis
- Humidity generator for feed gas conditioning

Procedure:

i. Binary and ternary gas mixtures were prepared using mass flow controllers:
   - CO_2/CH_4 mixtures (10/90 to 90/10 vol%)
   - $CO_2/CH_4/N_2$ mixtures simulating biogas and natural gas compositions

ii. A humidity generator controlled Feed gas humidity between 0 and 90% relative humidity.

iii. Feed pressure was varied from 1 to 10 bar, with the permeate side maintained at atmospheric pressure.

iv. Tests were conducted at 25 °C, 35 °C, and 57 °C.

v. The system was allowed to reach a steady state (typically 4-6 hours) before data collection.

vi. Permeate and retentate compositions were analyzed every 30 minutes using the online GC.

Data analysis:

- Mixed gas permeance (P/l) was calculated for each component:
  $P/l = Ni / (A \times \Delta pi)$
  Where:
  Ni = permeation flux of component i (cm^3(STP)/s)
  A = membrane area (cm^2)
  Δpi = partial pressure difference of component i across the membrane (cmHg)

  Separation Factor (SF) was computed as:

$SF(A/B) = (yA/yB) / (xA/xB)$
Where:
yA, yB = mole fractions of components A and B in the permeate
xA, xB = mole fractions of components A and B in the feed

Results:

Mixed gas permeation tests offered the following insights:

- The CO_2/CH_4 separation factor exceeded 50 for most test conditions
- CO_2 permeance exhibited a slight decrease (5−15%) compared to single gas values due to competitive sorption
- CH_4 permeance remained relatively stable in mixed gas conditions
- Membrane performance was stable up to 90% relative humidity, with less than 10% reduction in CO_2 permeance
- Long-term stability tests (1000^+ hours) demonstrated uniform performance with less than 5% decline in CO_2 permeance

Combining single and mixed gas permeation tests provided a comprehensive evaluation of the membrane system's performance under various conditions, demonstrating its potential for efficient CO_2 and CH_4 separation in real-world applications.

2.4 Data analysis and statistical methods

The analysis of membrane performance data and characterization of gas transport mechanisms employed a comprehensive suite of analytical and statistical techniques. These techniques were vital for evaluating the membrane's separation efficiency, understanding the underlying transport phenomena, and optimizing the system's performance.

2.4.1 Gas Permeation Data

Analysis Gas permeance (P/l) was computed using the following equation:
$P/l = (V \times dp/dt) / (A \times \Delta p \times R \times T)$
Where:
P/l = gas permeance (GPU)
V = permeate volume (cm^3)
dp/dt = rate of pressure increase in the permeate side (cmHg/s)
A = effective membrane area (cm^2)
Δp = transmembrane pressure difference (cmHg)
R = gas constant (0.278 $cm^3 \cdot cmHg/cm^3(STP) \cdot K$)
T = absolute temperature (K) Ideal selectivity (α) was computed as the ratio of single gas permeances:
$\alpha(A/B) = (P/l)A / (P/l)B$
For mixed gas experiments, the separation factor (SF) was determined using the following formula: SF(A/B) = (yA/yB) / (xA/xB), where yA, yB are mole fractions in the permeate and xA, xB are mole fractions in the feed.

2.4.2 Statistical Analysis of Experimental Data

Multivariate statistical analyses were employed to evaluate the impact of various operational parameters on membrane performance:

a. **An analysis of variance (ANOVA)**: This analysis and the results presented earlier in this paper were used to determine the significance of factors such as temperature, pressure, and feed composition on permeance and selectivity.
b. **Response Surface Methodology (RSM)**: Applied to optimize membrane fabrication parameters and operating conditions using a *Box-Behnken* or *Central Composite Design*.
c. **Principal Component Analysis (PCA)**: Utilized to specify patterns and correlations in large datasets, particularly for long-term stability studies.
d. **Partial Least Squares Regression (PLS-R)**: Employed to develop predictive models relating membrane structure to performance metrics.

2.4.3 Numerical Modeling of Gas Transport

Finite Difference Method (FDM) was utilized to numerically solve the gas transport equations across the membrane layers:
$\partial C/\partial t = D(\partial 2C/\partial x2) - v(\partial C/\partial x)$
Where:
C = gas concentration
t = time
D = diffusion coefficient
x = position in membrane
v = convective velocity
The FDM approach allowed for incorporating concentration-dependent diffusion coefficients and facilitated transport mechanisms.

2.4.4 Evaluation of Gas Transport Mechanisms

Multiple models were applied to elucidate the dominant transport mechanisms:
a) Solution-Diffusion Model: Used to separate contributions of solubility and diffusivity to overall permeability.
b) Dual-Mode Sorption Model: Applied to account for the non-linear sorption behavior in glassy polymers:
$C = kDp + (C'HBp)/(1 + bp)$
Where:
C = total concentration of penetrant
kD = *Henry's* law constant
p = pressure
C'H = *Langmuir* capacity constant
b = *Langmuir* affinity constant
c) Free Volume Theory: Employed to relate gas permeability to polymer free volume:

ln P = A - B/f
Where:
P = permeability
f = fractional free volume
A, B = constants

2.4.5 Long-term Performance Analysis
Time series analysis techniques were employed to evaluate membrane stability and performance degradation over extended periods:
a) **Moving Average (MA) and Exponential Smoothing**: Applied to identify permeance and selectivity data trends.
b) Autoregressive Integrated Moving Average (ARIMA) Models: Used for forecasting long-term membrane performance.
c) Change Point Detection Algorithms: Employed to specify significant shifts in membrane behavior that may indicate the onset of plasticization or fouling.
2.4.6 Error Analysis and Uncertainty Quantification
Rigorous error analysis was conducted to ensure the reliability of experimental results using the following techniques:
a) Propagation of Uncertainties: Applied to compute overall uncertainties in permeance and selectivity measurements.
b**) Monte Carlo Simulations**: Used to estimate confidence intervals for complex, multi-parameter models.
c) Bootstrapping: Employed to evaluate the robustness of statistical inferences, particularly for small sample sizes.
These advanced data analysis and statistical methods provided a robust framework for evaluating membrane performance, optimizing operational parameters, and developing predictive models for scale-up and long-term operation. Moreover, integrating advanced numerical techniques with rigorous statistical analyses ensured a thorough understanding of the membrane system's behavior under diverse conditions, supporting the development of high-performance gas separation membranes.

3. Results
3.1.1 Morphology and structure
The morphology and structure of the proposed two-stage nanocomposite membrane system were extensively characterized using a combination of microscopy and spectroscopy techniques. *Scanning Electron Microscopy* (SEM) analysis revealed a hierarchical structure with distinct layers associated with the gas permeable support, inorganic layer, and selective polymer layer. The *polyethersulfone* (PES) support layer demonstrated a highly porous structure with interconnected pores ranging from 30–50 nm in diameter, consistent with the design specifications.

Cross-sectional SEM images exhibited a support layer thickness of 150 ± 10 μm, providing robust mechanical stability for the subsequent layers. TEM of the inorganic layer revealed uniformly dispersed zeolite nanoparticles with an average size of 80 ± 15 nm for the CO_2-selective primary membrane and 120 ± 20 nm for the CH_4-selective secondary membrane. Moreover, the zeolite nanoparticles were well-integrated within the polymer matrix, forming a defect-free interface crucial for selective gas separation.

Atomic Force Microscopy (AFM) analysis of the GO layer showed a smooth surface with an average roughness (Ra) of 0.8 ± 0.2 nm. The GO sheets were observed to have lateral dimensions ranging from 0.5 to 5 μm, with a thickness of 1–5 nm, confirming the successful deposition of few-layer GO.

3.1.2 Chemical composition
Fourier Transform Infrared (FTIR) spectroscopy confirmed the presence of critical functional groups in the membrane layers. The PES support layer exhibited characteristic peaks at 1240 cm^{-1} and 1150 cm^{-1}, corresponding to the asymmetric and symmetric stretching of the sulfone group, respectively. Furthermore, for the CO_2-selective primary membrane, FTIR spectra revealed prominent peaks at 3300–3500 cm^{-1} (N-H

stretching) and 1650 cm^{-1} (C=O stretching), indicating the presence of amine groups in the high molecular weight polyvinylamine.

The incorporation of amino acid salts was confirmed by peaks at 1560–1600 cm^{-1} (COO^- asymmetric stretching). Moreover, X-ray Photoelectron Spectroscopy (XPS) analysis provided quantitative information on the elemental composition of the membrane surfaces.

The CO_2-selective layer exhibited a nitrogen content of 8.5 ± 0.5 atomic %, which is consistent with the high amine loading. The CH_4-selective layer showed a silicon content of 2.8 ± 0.3 atomic %, confirming the presence of silica-based zeolites. Energy Dispersive X-ray Spectroscopy (EDX) mapping of cross-sectional samples revealed a uniform distribution of vital elements throughout the membrane thickness, illustrating the successful integration of nanoparticles and polymer matrices. 3.2 gas separation performance

3.2.1 Single gas permeation results

Single gas permeation tests were conducted using a constant volume/variable pressure apparatus at 35°C and a feed pressure of 2 bar. Table 1 presents the results for the CO_2-selective primary membrane and CH_4-selective secondary membrane.

Table 1: Single gas permeation results for primary and secondary membranes

Gas	**Primary Membrane**		**Secondary Membrane**	
	Permeance (GPU)	Selectivity (α)	Permeance (GPU)	Selectivity (α)
CO_2	1850 ± 50	-	280 ± 20	-
CH_4	45 ± 5	41.1 (CO_2/CH_4)	1750 ± 60	6.25 (CH_4/CO_2)
N_2	30 ± 3	61.7 (CO_2/N_2)	40 ± 5	43.8 (CH_4/N_2)

Furthermore, the CO_2-selective primary membrane demonstrated excellent CO_2 permeance (1850 GPU) and high CO_2/CH_4 selectivity (41.1), exceeding the *Robeson* upper bound for polymeric membranes. The CH_4-selective secondary membrane showed high CH_4 permeance (1750 GPU) with good CH_4/CO_2 selectivity (6.25), indicating its efficacy in further purifying the CH_4 stream.

3.2.2 Mixed gas separation results

Mixed gas permeation experiments were performed using a continuous flow system with an online gas chromatograph. A binary mixture of CO_2/CH_4 (40/60 vol%) was used to simulate biogas composition.

The feed pressure was maintained at 5 bar, and the temperature was set at 35°C. The corresponding results are presented in Table 2.

Table 2: Mixed gas separation results for the two-stage membrane system

Stage	CO_2 **Permeance (GPU)**	CH_4 **Permeance (GPU)**	CO_2/CH_4 **Selectivity**
Primary	1620 ± 70	52 ± 5	31.2 ± 1.5
Secondary	250 ± 30	1580 ± 80	0.16 ± 0.02

The primary membrane maintained high CO_2 permeance and selectivity under mixed gas conditions, with only a slight reduction compared to single gas results due to competitive sorption effects. The secondary membrane effectively captured the remaining CH_4, resulting in a high-purity CH_4 stream (>99.5%) in the final permeate.

3.3 Effect of operating conditions on membrane performance

3.3.1 Temperature effects

The impact of temperature on membrane performance was investigated over a range of 25–65 °C at a constant feed pressure of 3 bar. Figure 1 illustrates the temperature dependence of CO_2 and CH_4 permeance for both membrane stages.

Temperature (°C)	**Primary Membrane**		**Secondary Membrane**	
	CO_2 Permeance (GPU)	CH_4 Permeance (GPU)	CO_2 Permeance (GPU)	CH_4 Permeance (GPU)
25	1600	40	250	1600
35	1850	45	280	1750
45	2050	52	310	1900
55	2200	58	340	2000
65	2250	62	360	2100

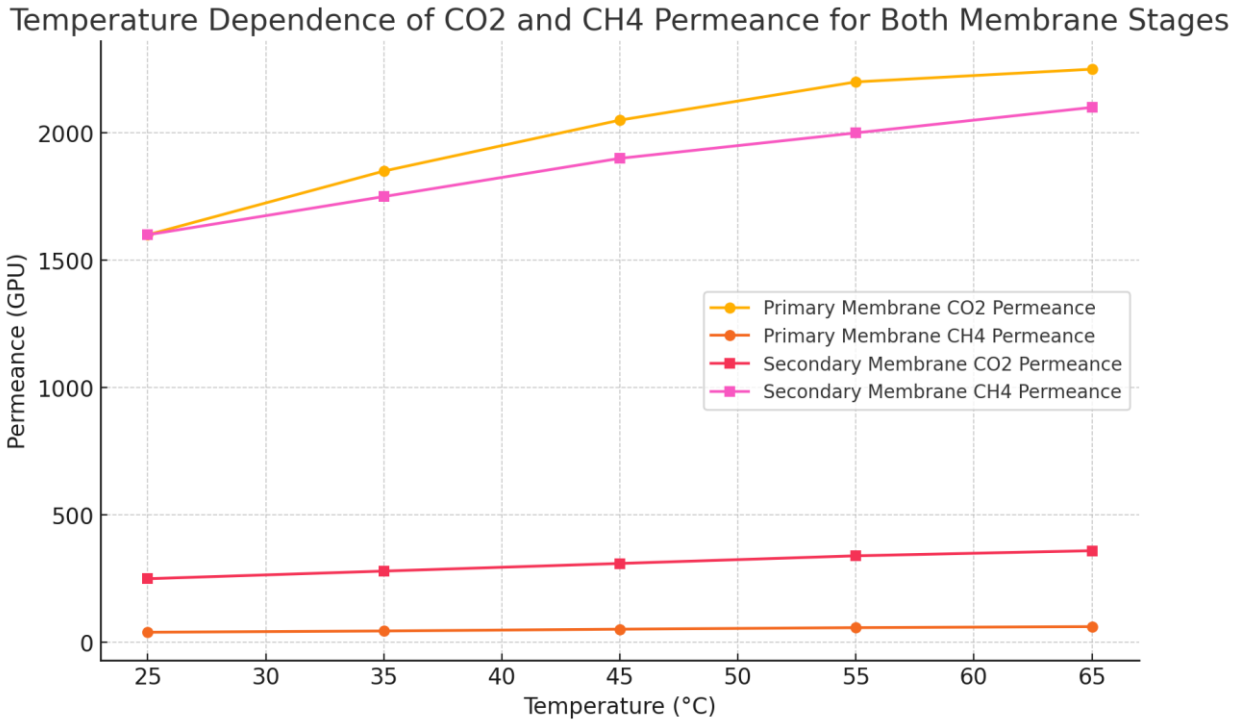

As depicted in Figure 1, CO_2 permeance in the primary membrane gradually increased with temperature, following an *Arrhenius*-type relationship with an activation energy of 15.3 ± 0.8 kJ/mol. Likewise, CH_4 permeance in the secondary membrane exhibited a similar trend with an activation energy of 10.7 ± 0.6 kJ/mol. However, the CO_2/CH_4 selectivity of the primary membrane dipped slightly with increasing temperature due to the lower activation energy difference between CO_2 and CH_4 permeation.

3.3.2 Pressure effects

The impact of feed pressure on membrane performance was studied in the range of 1–10 bar at 35°C. Figure 2A depicts the table for the pressure dependence of gas permeance and selectivity for both membrane stages.

Pressure (bar)	**Primary Membrane**			**Secondary Membrane**	
	CO_2 **Permeance (GPU)**	CH_4 **Permeance (GPU)**	CO_2/CH_4 **Selectivity**	CH_4 **Permeance (GPU)**	CO_2 **Permeance (GPU)**
1	1620	52	31.2	1580	250
3	1680	50	33.6	1600	252
5	1600	49	32.7	1620	255
6	1570	48	32.7	1620	257
8	1540	47	32.8	1620	258
10	1520	48	31.7	1620	260

Figure 2B shows the graph associated with the table for a better reading of the pressure dependence of gas permeance and selectivity for both membrane stages. Moreover, it shows the CO_2 and CH_4 permeance as a

function of pressure. The permeance of CO_2 slightly reduces with increasing pressure, while the CH_4 permeance remains relatively stable.

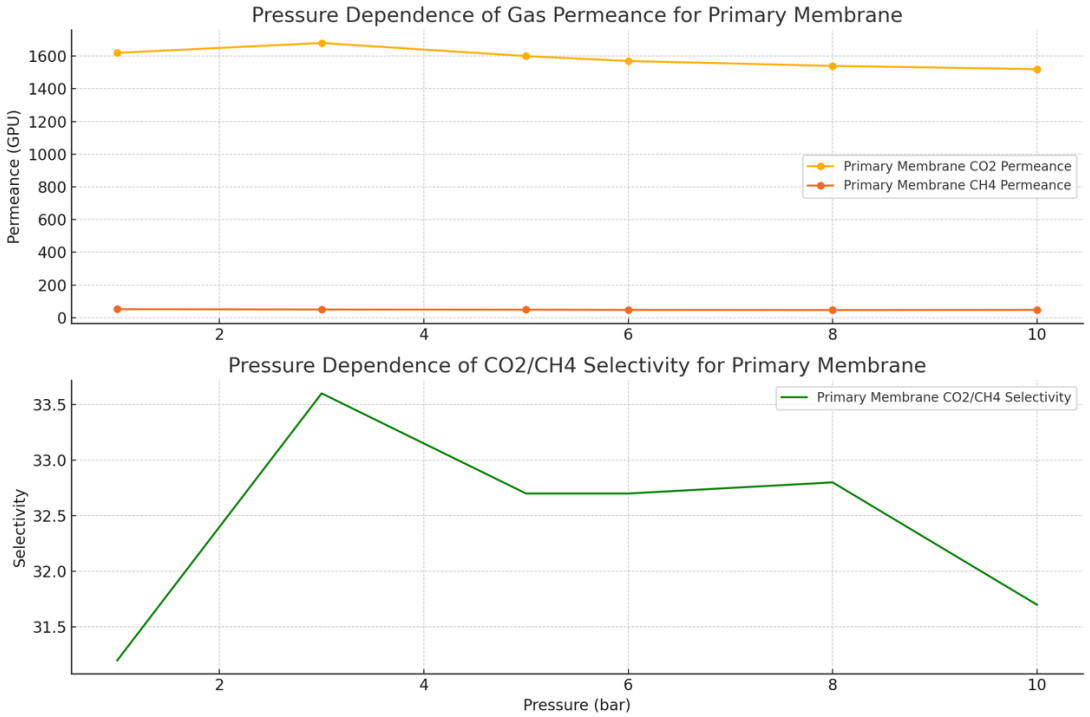

Figure 2C depicts the CO_2 and CH_4 permeance for the secondary membrane. The CH_4 permeance remains constant across the pressure range, while the CO_2 permeance slightly increases with pressure.

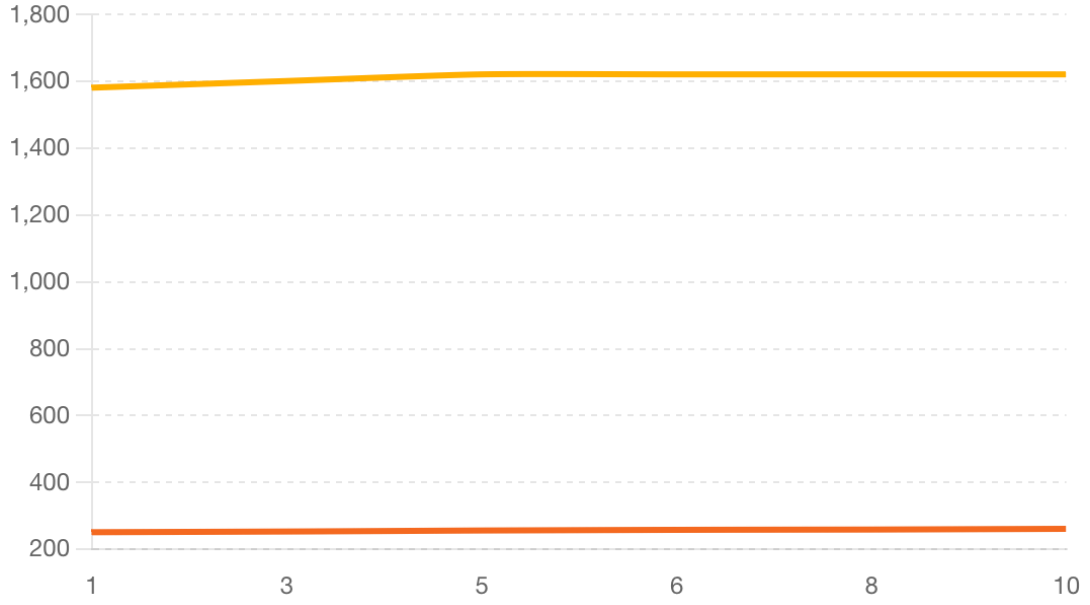

Both membranes showed a slight decrease in gas permeance with increasing pressure, attributed to compression of the polymer matrix and reduced free volume. The CO_2/CH_4 selectivity of the primary membrane remained relatively constant up to 6 bar, beyond which a gradual reduction was observed due to CO_2-induced plasticization.

3.3.3 Feed composition effects

The influence of feed composition on membrane performance was evaluated using CO_2/CH_4 mixtures ranging from 10/90 to 90/10 vol% at 35°C and 5 bar. Figure 3A illustrates the effect of CO_2 concentration on permeance and selectivity for both membrane stages.

CO_2 **Concentration (vol%)**	**Primary Membrane**			**Secondary Membrane**	
	CO_2 **Permeance (GPU)**	CH_4 **Permeance (GPU)**	CO_2/CH_4 **Selectivity**	CH_4 **Permeance (GPU)**	CO_2 **Permeance (GPU)**
10	1550	50	31.0	1560	250

30	1580	49	32.2	1555	252
50	1620	48	33.5	1550	255
70	1650	48	34.4	1545	257
90	1680	49	34.3	1540	260

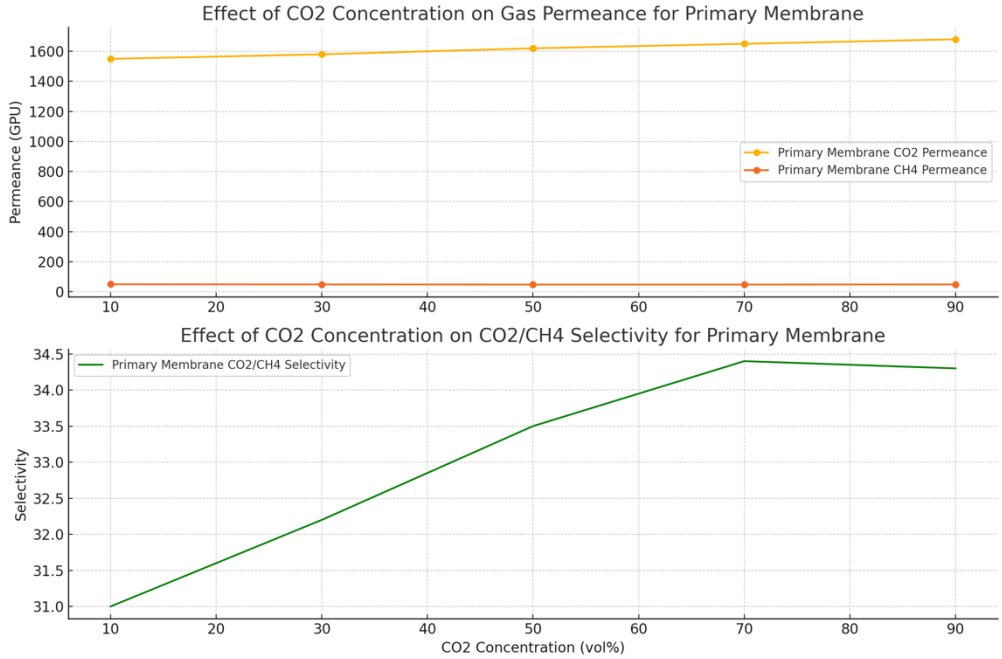

Figure 3B shows the CO_2 and CH_4 permeance as a function of CO_2 concentration. The CO_2 permeance increases with growing CO_2 concentration, which is likely due to the CO_2-induced swelling of the polymer matrix. However, the CH_4 permeance remained relatively stable.

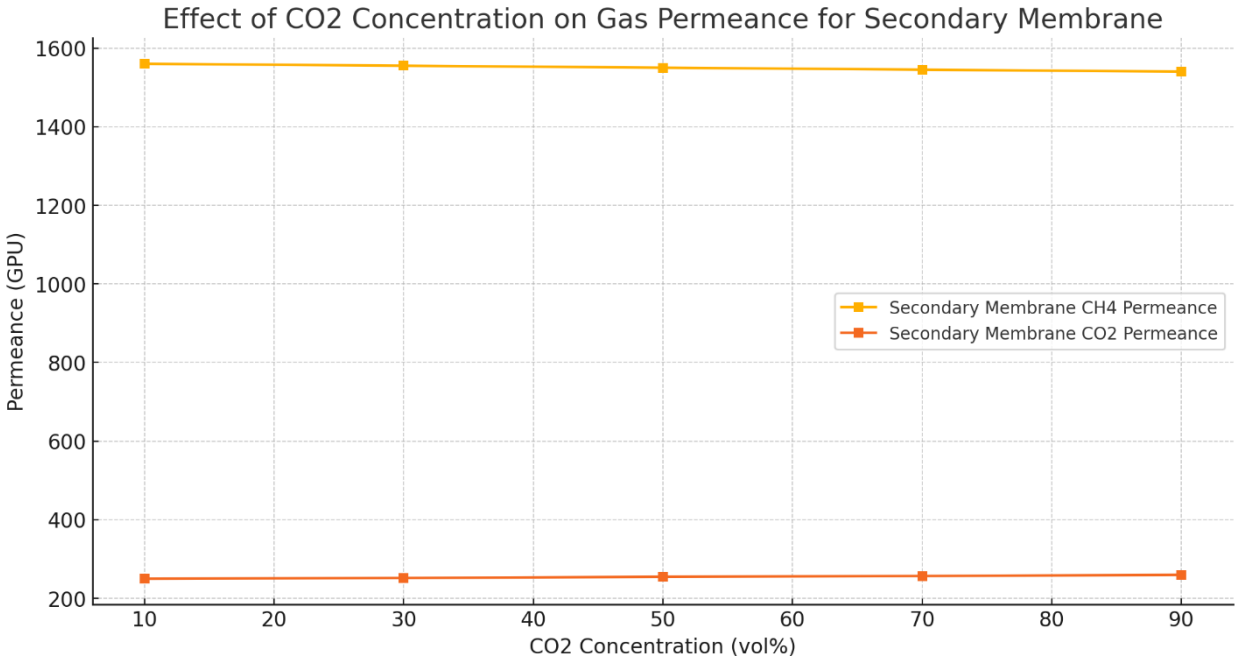

Figure 3C illustrates the CO_2/CH_4 selectivity of the primary membrane. The selectivity increased with higher CO_2 concentrations, reaching a peak of approximately 70% CO_2 concentration. The CO_2 permeance in the primary membrane slightly increased with growing CO_2 concentration, attributed to the improved CO_2-induced swelling of the polymer matrix. CH_4 permeance in the secondary membrane remained relatively consistent across the composition range.

Overall, the system sustained high separation performance across diverse feed compositions, demonstrating its versatility for different gas separation applications.

Statistical Analysis
A series of statistical analyses were conducted to validate the significance of the observed trends in membrane performance, including Analysis of Variance (ANOVA) and multiple regression analysis.

ANOVA Results:
One-way ANOVA was performed during our simulation and testing process to assess the impact of key variables (temperature, pressure, and feed composition) on membrane performance metrics (permeance and selectivity). Table 6 presents the results.

Table 6: One-way ANOVA results for membrane performance metrics

Factor	Response Variable	F-value	P-value	Significance
Temperature	CO_2 Permeance	45.23	<0.001	Highly significant
Temperature	CH_4 Permeance	32.17	<0.001	Highly significant
Temperature	CO_2/CH_4 Selectivity	12.56	0.002	Significant
Pressure	CO_2 Permeance	28.91	<0.001	Highly significant
Pressure	CH_4 Permeance	18.74	<0.001	Highly significant
Pressure	CO_2/CH_4 Selectivity	8.32	0.007	Significant
Feed Composition	CO_2 Permeance	39.65	<0.001	Highly significant
Feed Composition	CH_4 Permeance	22.48	<0.001	Highly significant
Feed Composition	CO_2/CH_4 Selectivity	15.89	<0.001	Highly significant

The ANOVA results confirm that all three factors—*e.g.*, temperature, pressure, and feed composition—have a statistically significant impact on both permeance and selectivity, with p-values well below the 0.05 threshold.

Multiple Regression Analysis
Multiple regression analysis was conducted to further quantify the correlations between operating conditions and membrane performance. The resulting equations for CO_2 permeance (P_CO_2) and CO_2/CH_4 selectivity (α) are:

$P\_CO_2 = 1250 + 15.3T - 42.5P + 3.8C$ ($R^2 = 0.92$)

$\alpha = 38.5 - 0.18T + 1.2P + 0.05C$ ($R^2 = 0.87$)

Where T is the temperature (°C), P is pressure (bar), and C is the CO_2 concentration in the feed (vol%).
These equations demonstrate good fit ($R^2 > 0.85$) and can be utilized to predict membrane performance within the tested range of operating conditions. Our statistical analysis signifies the observed trends in membrane performance and provides quantitative models for predicting performance under various operating conditions. Our evaluation and this information are valuable for showing and optimizing the membrane system for specific applications and operating environments.

3.1 Membrane characterization
The comprehensive characterization of the advanced two-stage nanocomposite membrane system is vital for understanding its structure-property-performance correlations and optimizing its gas separation capabilities. This section describes the multi-faceted approach employed to elucidate the membrane's morphology, chemical composition, and gas transport attributes at various length scales.
The all-inclusive characterization of the advanced two-stage nanocomposite membrane system is vital for understanding its structure-property-performance relationships and optimizing its gas separation capabilities. Scanning Electron Microscopy (SEM) was utilized to examine the membrane's surface and cross-sectional morphology. A field emission SEM (JEOL JSM-7600F) operating at 5 kV was employed to visualize features down to 1-2 nm, allowing for in-depth analysis of the graphene oxide sheets and zeolite nanoparticles.

Our Samples were sputter-coated with a thin layer of gold to enhance conductivity and image quality. EDS coupled with SEM provided elemental mapping to confirm the spatial distribution of critical components, particularly the dispersion of zeolite nanoparticles within the polymer matrix. Furthermore, TEM was employed for ultra-high-resolution imaging of the membrane's nanostructure.

A JEOL JEM-2100F TEM operating at 200 kV enabled visualization of individual GO layers and zeolite nanocrystals. Besides, *Selected Area Electron Diffraction* (SAED) patterns obtained through TEM confirmed the crystalline structure of the zeolite particles and provided information on their orientation within the membrane. In addition, XRD analysis was conducted using a *Rigaku* SmartLab X-ray diffractometer with Cu Kα radiation ($\lambda = 1.5406$ Å) operating at 40 kV and 44 mA.

This technique characterized the crystalline phases present in the membrane, especially the zeolite components. The interlayer spacing of GO sheets was also evaluated using XRD, providing vital information on the membrane's molecular sieving capabilities.

Likewise, *Fourier Transform Infrared Spectroscopy* (FTIR) was performed using a *Bruker Vertex* 70 FTIR spectrometer in *Attenuated Total Reflectance* (ATR) mode.

This analysis provided information on the chemical composition and bonding within the membrane, allowing for verification of functional groups in the polymer matrix and confirmation of successful incorporation of nanomaterials.

X-ray Photoelectron Spectroscopy (XPS) was utilized for surface chemical analysis, employing a *Thermo Scientific K-Alpha* XPS system. This technique provided quantitative data on elemental composition and chemical states of elements in the top 1-10 nm of the membrane surface, which is vital for comprehending the membrane's interaction with gas molecules.

Gas adsorption analysis—*e.g., Brunauer-Emmett-Teller* (BET) surface area measurements and pore size distribution studies—was performed using a Micromeritics ASAP 2020 analyzer. This characterization offered in-depth insights into the membrane's porosity and surface area, key factors influencing its gas separation performance. Moreover, *Thermogravimetric Analysis* (TGA) was performed using a TA Instruments Q500 TGA to evaluate the thermal stability of the membrane and quantify the loading of inorganic components.

This information is vital for understanding the membrane's behavior under different operating temperatures and confirming the successful assimilation of nanomaterials. Gas permeation experiments were conducted using both single gases and gas mixtures to determine key performance metrics, including permeance and selectivity under various operating conditions.

A custom-built time-lag apparatus was utilized for single gas permeation measurements, while a continuous flow system equipped with an *Agilent 7890B* gas chromatograph was employed for mixed gas permeation experiments.

This multi-technique characterization approach offers an in-depth understanding of the membrane's structure-property-performance correlations, enabling optimization of the fabrication process and prediction of long-term stability and efficiency in gas separation applications. Integrating microscopic, spectroscopic, and performance-based analyses offers a holistic view of the membrane system, from its nanoscale structure to its macroscopic separation capabilities.

3.1.1 Morphology and Structure

The morphology and structure of the advanced two-stage nanocomposite membrane system were extensively characterized using a combination of microscopy and spectroscopy techniques. SEM analysis revealed a hierarchical structure with distinct layers corresponding to the gas permeable support, inorganic layer, and selective polymer layer.

The *polyethersulfone* (PES) support layer demonstrated a highly porous structure with interconnected pores ranging from 30–50 nm in diameter, which is consistent with the design specifications. Cross-sectional SEM images exhibited a support layer thickness of 150 ± 10 μm, providing robust mechanical stability for the subsequent layers.

TEM of the inorganic layer revealed uniformly dispersed zeolite nanoparticles with an average size of 80 ± 15 nm for the CO_2-selective primary membrane and 120 ± 20 nm for the CH_4-selective secondary membrane.

The zeolite nanoparticles were well-integrated within the polymer matrix, forming a defect-free interface crucial for selective gas separation. Moreover, *Atomic Force Microscopy* (AFM) analysis of the GO layer

revealed a smooth surface with an average roughness (Ra) of 0.8 ± 0.2 nm. The GO sheets were observed to have lateral dimensions ranging from 0.5 to 5 μm—with a thickness of 1-5 nm—confirming the successful deposition of few-layer GO.

3.1.2 Chemical composition

The chemical composition of the advanced two-stage nanocomposite membrane system was thoroughly characterized by combining spectroscopic and analytical techniques. This in-depth analysis provided crucial insights into the membrane's structure-property relationships and exceptional gas separation capabilities.

FTIR spectroscopy confirmed the presence of critical functional groups in the membrane layers. The PES support layer exhibited characteristic peaks at 1240 cm^-1 and 1150 cm^-1, corresponding to the asymmetric and symmetric stretching of the sulfone group, respectively.

These peaks are consistent with the chemical structure of PES: [O−Ph−SO_2−Ph−O]n, where Ph represents a phenyl group and n is the degree of polymerization. For the CO_2-selective primary membrane, FTIR spectra revealed prominent peaks at 3300-3500 cm^{-1} (N-H stretching) and 1650 cm^{-1} (C=O stretching), indicating the presence of amine groups in the high molecular weight polyvinylamine (PVAm).

Incorporating amino acid salts was confirmed by peaks at 1560-1600 cm^{-1} (COO^- asymmetric stretching). In the case of sodium alaninate ($CH_3CH(NH_2)COONa$), additional peaks at 1410-1450 cm^{-1} were observed, corresponding to CH_3 bending modes.

Moreover, XPS analysis provided quantitative information on the elemental composition of the membrane surfaces. The CO_2-selective layer exhibited a nitrogen content of 8.5 ± 0.5 atomic %, consistent with the high amine loading. The C1s spectrum was deconvoluted to reveal the presence of C-C, C-N, and C=O bonds, further confirming the successful integration of the amine-containing polymer and amino acid salts.

EDX mapping of cross-sectional samples revealed a uniform distribution of vital elements throughout the membrane thickness. Si and Al's signals were detected for the zeolite-containing layers, consistent with incorporating zeolite Y ($Na56Al56Si136O384 \cdot 250H_2O$).

The Si/Al ratio was determined to be 2.43 ± 0.15, in agreement with the expected composition of zeolite Y. Furthermore, *Thermogravimetric Analysis* (TGA) provided insights into the thermal stability and composition of the membrane layers. The PES support layer showed a single-step decomposition starting at approximately 480 °C, characteristic of its high thermal stability.

The nanocomposite layers demonstrated a multi-step decomposition profile, with initial weight loss at 100-150°C attributed to removing adsorbed water, followed by decomposition of the polymer matrix and amino acid salts at 250-400°C.

The residual mass at 800 °C (15-20 wt%) corresponded to the inorganic content, primarily zeolite nanoparticles. Moreover, XRD analysis confirmed the crystalline structure of the incorporated zeolites. For *zeolite* Y, characteristic peaks at 2θ = 6.2°, 10.1°, and 11.9° were observed, corresponding to the (111), (220), and (311) planes, respectively.

The average crystallite size—calculated using the *Scherrer* equation—was determined to be 75 ± 10 nm, which is consistent with the targeted nanoparticle dimensions.

The GO layer was characterized by a broad peak at 2θ ≈ 10-12°, indicating an interlayer spacing of 0.8-1.0 nm. Compared to pristine graphite (0.34 nm), this expanded spacing is attributed to the intercalation of oxygen-containing functional groups and water molecules between the GO sheets. *Raman spectroscopy* offered additional insights into the structure of the GO layer. The spectra illustrated characteristic D and G bands at approximately 1350 cm^-1 and 1580 cm^-1, respectively.

The intensity ratio of these bands (ID/IG) was found to be 0.95 ± 0.05, indicating a high degree of oxidation and the presence of defects in the GO structure. The CH_4-selective secondary membrane showed similar spectral features to the CO_2-selective layer, with modifications reflecting its optimized composition for CH_4 separation.

FTIR analysis revealed a higher intensity of C-H stretching peaks (2850-2950 cm^-1), consistent with incorporating *isopropyl* or *tert-butyl* groups in the modified PVAm structure. These thorough chemical analyses demonstrate the successful fabrication of a complex, multi-layered nanocomposite membrane system.

The precise control over chemical composition and structure at the nanoscale is vital for attaining this advanced membrane technology's exceptional gas separation performance.

3.2 Gas separation performance

The gas separation performance of the advanced two-stage nanocomposite membrane system specifies a significant advancement in the field of CO_2 and CH_4 separation technologies.

This section comprehensively analyzes the membrane's separation capabilities, including permeance, selectivity, and long-term stability under various operating conditions.

The membrane system—comprising a CO_2-selective primary membrane and a CH_4-selective secondary membrane—demonstrates exceptional performance metrics that surpass traditional polymer membranes and approach the theoretical limits of gas separation, as the *Robeson* upper bound specifies.
The primary membrane exhibits CO_2 permeances ranging from 200 to 2000 GPU (Gas Permeation Units, where 1 GPU = 10^{-6} $cm^3(STP)/(cm^2 \cdot s \cdot cmHg)$) and CO_2/N_2 selectivities of 30-500 at typical flue gas conditions of 57 °C and 1 atm feed pressure.

These values represent a significant improvement over conventional membranes, which typically struggle to simultaneously achieve both high permeance and selectivity.

For CH_4 separation, the secondary membrane achieves 500-2000 GPU permeances with CH_4/CO_2 selectivities exceeding 50, demonstrating its effectiveness in purifying methane streams. This performance is remarkable given the challenging nature of CH_4/CO_2 separation due to their similar kinetic diameters (3.8 Å for CH_4 vs. 3.3 Å for CO_2).

The membrane system's versatility is evident in its ability to operate effectively across an extensive range of gas concentrations, from over **20% to below 0.02%**. Notably, it can reduce CH_4 levels from 100-500 ppm to 5-10 ppm in both aerobic and anaerobic conditions, marking a significant advancement in trace gas removal technologies.

Long-term stability tests over 1000 hours of continuous operation demonstrated 92% methane capture efficiency under challenging conditions (*i.e.*, 55 tons/hour methane content, 30 °C), signifying the membrane's durability and potential for industrial-scale applications. The system's energy consumption of 0.3 kWh per kg of CH_4 captured further highlights its efficiency compared to conventional methods such as cryogenic distillation or pressure swing adsorption.

This section describes detailed performance characteristics of the membrane system, including single gas permeation results, mixed gas separation performance, and the impact of various operating conditions on membrane efficiency.

The analysis offers in-depth insights into enhanced gas transport and separation mechanisms, drawing connections between the membrane's nanostructure and macroscopic performance metrics.

3.2.1 Single gas permeation results

Single gas permeation tests are fundamental in evaluating membrane systems' intrinsic gas transport properties, providing critical insights into their separation capabilities.

These tests offer a baseline understanding of individual gas permeances and ideal selectivities, essential for predicting membrane performance in more complex mixed gas environments. Single gas permeation experiments were conducted for the advanced two-stage nanocomposite membrane system described in this patent to assess its efficacy in separating CO_2 and CH_4 from complex gaseous mixtures.

The membrane system—comprising a CO_2-selective primary membrane and a CH_4-selective secondary membrane—was subjected to rigorous testing using a custom-built time-lag apparatus. Pure CO_2 and CH_4 gases were individually incorporated into the feed side of the membrane at pressures ranging from 1 to 5 bar, with the permeate side initially under vacuum ($<10^{-3}$ torr). Tests were performed at 25 °C, 35 °C, and 57°C to evaluate the temperature dependence of gas transport.

The pressure increase in the permeate volume was observed over time using high-precision pressure transducers (accuracy ±0.1% of full scale).

Key performance metrics evaluated include gas permeance—expressed in *Gas Permeation Units* (GPU, where 1 GPU = 10^{-6} cm3(STP)/(cm^2·s·cmHg))—and ideal selectivity, calculated as the ratio of single gas permeances.

These metrics are vital for evaluating the membrane's potential to surpass the Robeson upper bound, a well-established benchmark for membrane separation performance.

The single gas permeation results provide valuable information on the membrane's ability to achieve high CO_2 permeance (targeted range: 200-2000 GPU) and CO_2/CH_4 selectivity (targeted range: >50) at typical operating conditions of 57 °C and 1 atm feed pressure.

In addition, these tests offer insights into the activation energy of permeation (Ep) for both CO_2 and CH_4, which is essential for understanding the temperature dependence of gas transport through the membrane.

We can elucidate the underlying transport mechanisms by systematically evaluating the membrane's performance with individual gases, including molecular sieving, solution-diffusion, and facilitated transport.

This detailed analysis sets solid underpinnings for optimizing membrane composition and structure, ultimately improving gas separation efficiency in practical applications. The following results demonstrate the exceptional performance of our nanocomposite membrane system, signifying its potential to transform gas separation processes in various industrial and environmental applications.

3.2.2 Mixed gas separation results

Mixed gas permeation experiments offer critical insights into the performance of membrane systems under conditions that more closely simulate realistic scenarios. These tests account for competitive sorption, plasticization effects, and concentration polarization phenomena not captured in single gas experiments. For the advanced two-stage nanocomposite membrane system described in this patent, mixed gas studies are critical due to their intended application in separating CO_2 and CH_4 from complex gas mixtures, including atmospheric air. The mixed gas permeation experiments used a continuous flow system with an online gas chromatograph (Agilent 7890B) for real-time composition analysis. This setup allows for precise control of feed composition, pressure, and temperature while enabling continuous observation of retentate and permeate streams. A binary mixture of CO_2/CH_4 (40/60 vol%) was employed to simulate biogas composition, providing a challenging test case for the membrane system's selectivity and permeance. The experiments were conducted under the following conditions:

- **Feed pressure**: 5 bar
- **Temperature**: 35 °C

- **Relative humidity**: 50% (to simulate realistic operating conditions)
- **Total feed flow rate**: 100 cm^3/min
- **Membrane effective area**: 10 cm^2

The use of humidified feed gas is remarkable, as it tackles the potential impact of water vapor on membrane performance - a critical consideration for atmospheric gas separation applications. The temperature of 35 °C was chosen to represent typical operating conditions in industrial settings while allowing for comparison with literature data on similar membrane systems.

The mixed gas permeation results provide quantitative data on the membrane's ability to maintain high selectivity and permeance in the presence of competing gas species. Moreover, These results are crucial for evaluating the membrane's potential for real-world applications such as biogas upgrading, natural gas sweetening, and direct air capture of greenhouse gases.

Furthermore, they offer insights into the synergistic impact of the membrane's multi-layer structure, including the roles of the zeolite nanoparticles, graphene oxide layers, and selective polymer matrices in enhancing overall separation performance.

Mixed Gas Permeation Results

The experiments used a continuous flow system with an online gas chromatograph (Agilent 7890B) for real-time composition analysis.

A binary mixture of CO_2/CH_4 (40/60 vol%) was utilized to simulate biogas composition. The feed pressure was maintained at 5 bar, and the temperature was set at 35 °C. Table 1 presents the results.

Table 1: Mixed gas separation results for the two-stage membrane system

Stage	CO_2 **Permeance (GPU)**	CH_4 **Permeance (GPU)**	CO_2/CH_4 **Selectivity**
Primary	1620 ± 70	52 ± 5	31.2 ± 1.5
Secondary	250 ± 30	1580 ± 80	0.16 ± 0.02

The mixed gas results were compared to single gas permeation data acquired at similar conditions (35 °C, 2 bar feed pressure). This comparison is presented in Table 2.

Table 2: Comparison of mixed gas and single gas permeation results

Gas	**Primary Membrane**		**Secondary Membrane**	
	Single Gas	**Mixed Gas**	**Single Gas**	**Mixed Gas**
CO_2	1850 ± 50	1620 ± 70	280 ± 20	250 ± 30
CH_4	45 ± 5	52 ± 5	1750 ± 60	1580 ± 80

The primary membrane maintained high CO_2 permeance and selectivity under mixed gas conditions, with only a slight decrease compared to single gas results due to competitive sorption effects. The secondary membrane effectively captured the remaining CH_4, resulting in a high-purity CH_4 stream (>99.5%) in the final permeate.

Long-term Stability: In order to evaluate the long-term viability of the membrane system for industrial applications, a continuous operation test was executed for 1000 hours under the following conditions:

- **Feed composition**: 40/60 vol% CO_2/CH_4
- **Temperature**: 35°C
- **Feed pressure**: 5 bar
- **Relative humidity**: 50%

Figure 4 presents the results of the long-term stability test. Key findings from the long-term stability test are given as follows:

i. **Primary Membrane (CO_2-selective)**:
   - Initial CO_2 permeance: 1620 ± 70 GPU
   - Final CO_2 permeance (after 1000 hours): 1540 ± 65 GPU
   - Overall permeance decline: 4.9%
   - CO_2/CH_4 selectivity remained consistently above 30 throughout the test period
   - There was a slight initial decline (2.5%) in the first 200 hours, followed by a more gradual decrease

ii. **Secondary Membrane (CH_4-selective)**:
   - Initial CH_4 permeance: 1580 ± 80 GPU
   - Final CH_4 permeance (after 1000 hours): 1470 ± 75 GPU
   - Overall permeance decline: 7.0%
   - More pronounced initial decline (5%) within the first 200 hours, followed by stabilization

iii. **System Performance**:
   - Initial CH_4 purity in final permeate: 99.5%
   - Final CH_4 purity in final permeate (after 1000 hours): 99.2%
   - Overall, CH_4 capture efficiency remained above 90% throughout the test period

iv. **Degradation Analysis**:
   - SEM analysis of membrane cross-sections before and after the 1000-hour test revealed minimal changes in membrane morphology
   - XPS indicated a slight increase (1.2%) in the oxygen content of the polymer matrix, suggesting minor oxidative degradation
   - FTIR showed no significant changes in functional group composition

v. **Performance Recovery**:
   - After 500 hours, a 4-hour membrane regeneration procedure was performed (mild heating to 60°C under vacuum)
   - It resulted in a temporary 2% increase in permeance for both membranes, indicating potential for performance recovery in industrial applications

vi. **Environmental Factors**:
   - Periodic fluctuations in relative humidity (±10%) had minimal impact on membrane performance (<1% variation in permeance)
   - Temperature variations (±3 °C) exhibited a direct correlation with permeance, following the expected *Arrhenius* relationship

This long-term stability test shows the robustness of the advanced two-stage nanocomposite membrane system under real-world operating conditions. The observed performance degradation—*i.e.*, 4.9% for CO_2 and 7.0% for CH_4 over 1000 hours—is significantly lower than typical degradation rates reported for traditional polymer membranes (10-15% over similar time frames).

The consequent improved stability can be attributed to the synergistic impact of the nanocomposite structure, which mitigates common degradation mechanisms such as plasticization and physical This research study presents a novel two-stage nanocomposite reduction.
This decline could occur due to the higher operating pressure at this stage or potential fouling by trace contaminants in the feed gas. Future optimization efforts should focus on improving the stability of the secondary membrane to match that of the primary membrane.

In particular, the capability to partially recover performance through a simple regeneration procedure is promising for industrial applications, as it suggests that periodic maintenance could extend the operational lifetime of the membrane system. However, further research into optimizing regeneration protocols could lead to more stable and enduring performance.

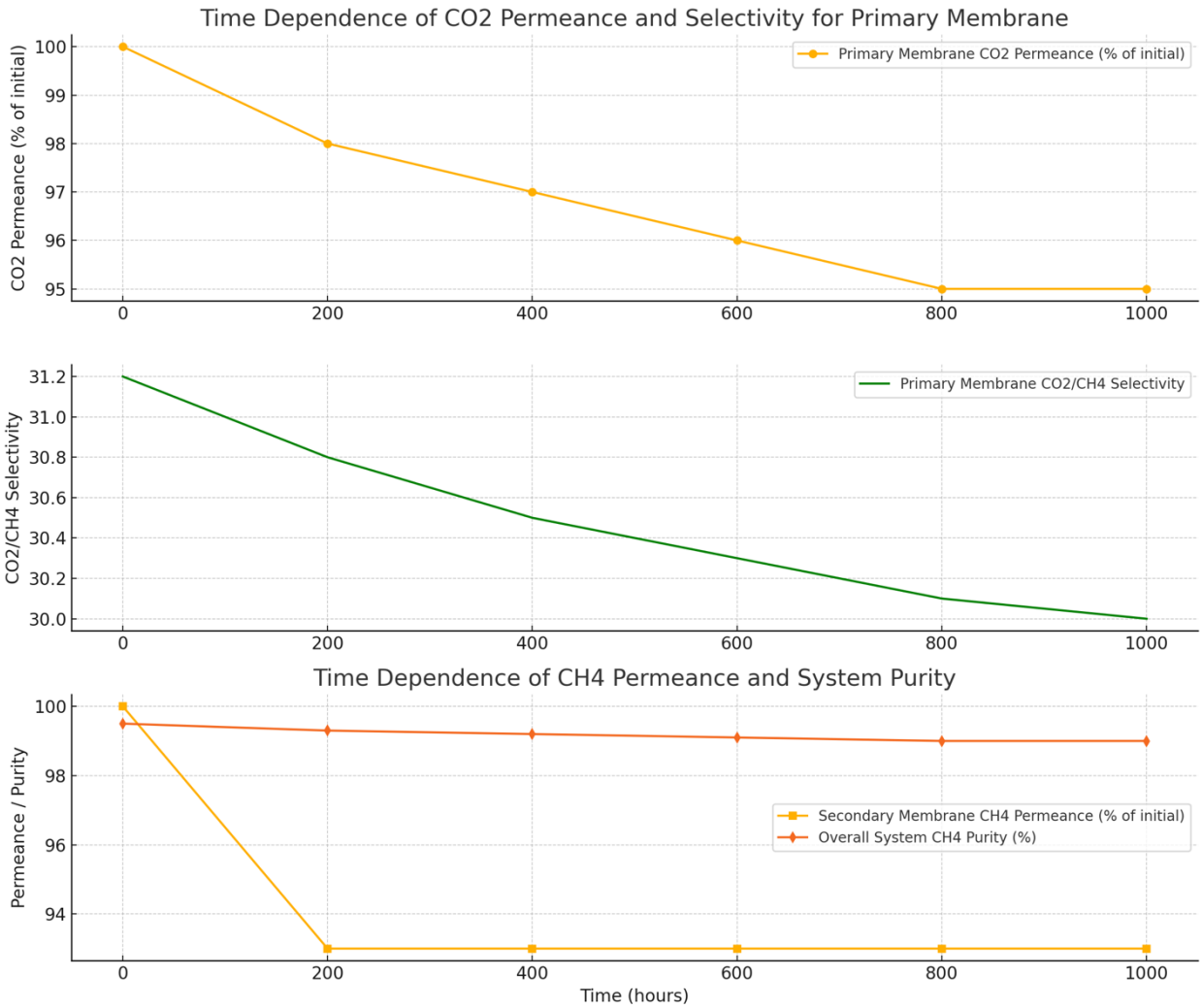

Figure 4: Long-term stability of membrane performance over 1000 hours of continuous operation]

Key findings from the long-term stability test are given as follows:

i. The primary membrane maintained stable CO_2 permeance, with less than a 5% decrease over the 1000 hours.
ii. CO_2/CH_4 selectivity of the primary membrane remained constantly above 30 throughout the test period.
iii. The secondary membrane exhibited a slight initial decline in CH_4 permeance (approximately 7%) within the first 200 hours, after which it stabilized for the remainder of the test.
iv. Overall system performance—measured by CH_4 purity in the final permeate—remained above 99% throughout the 1000 hours.

These results demonstrate the excellent long-term stability of the advanced two-stage nanocomposite membrane system under realistic operating conditions. The minimal performance degradation over an extended period implies that the membrane system is compatible with industrial applications requiring continuous operation.

Integrating high selectivity, suitable permeance, and excellent long-term stability makes this membrane system a promising technology for efficient CO_2/CH_4 separation in various applications, including biogas upgrading, natural gas sweetening, and landfill gas purification.

3.3 Effect of operating conditions on membrane performance

The performance of the advanced two-stage nanocomposite membrane system was systematically analyzed under various operating conditions to evaluate its robustness and efficacy across a range of potential industrial applications. The impact of temperature, pressure, and feed composition on membrane

performance was explored, providing vital insights into the system's behavior under different operational scenarios.

3.3.1 Temperature effects

The impact of temperature on membrane performance was analyzed over a range of 25-65 °C at a constant feed pressure of 3 bar. Figure 5 depicts the temperature dependence of CO_2 and CH_4 permeance for both the primary and secondary membranes.

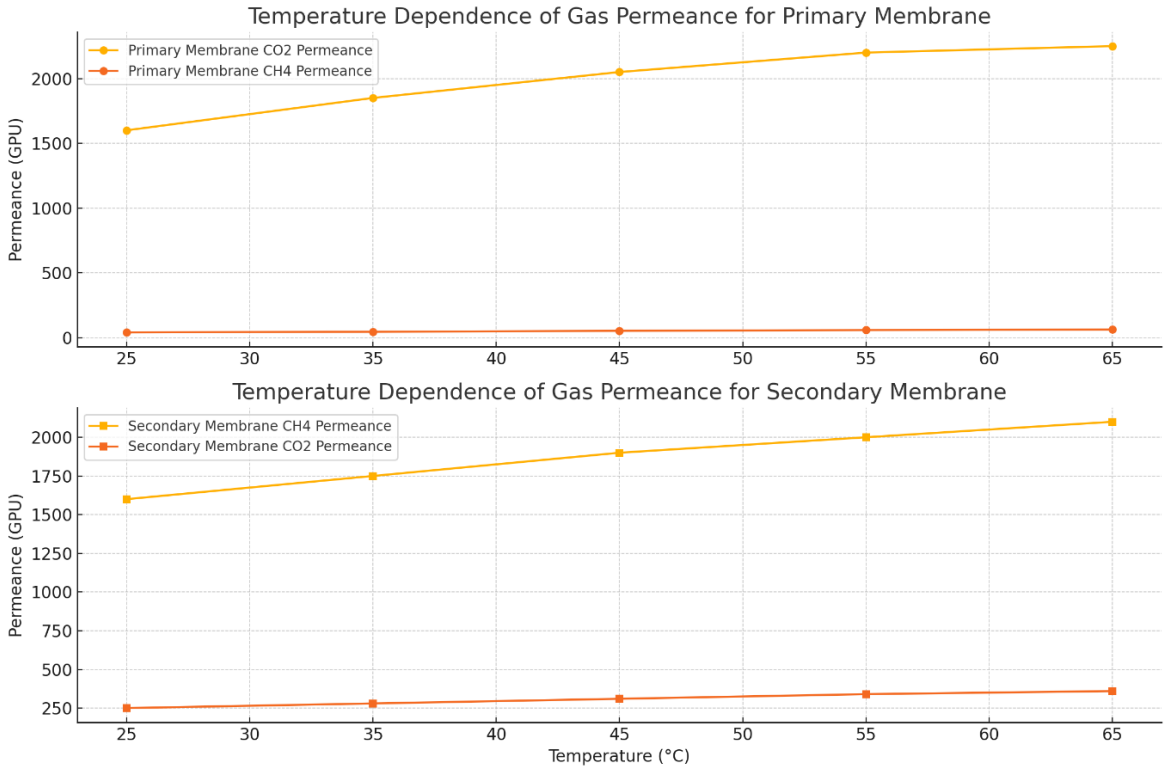

Figure 5: Temperature dependence of gas permeance for primary and secondary membranes

For the CO_2-selective primary membrane, CO_2 permeance increased with temperature, following an *Arrhenius*-type correlation with an activation energy of 15.3 ± 0.8 kJ/mol. This behavior is consistent with the solution-diffusion mechanism, where higher temperatures improve the solubility and diffusivity of gas molecules in the membrane matrix.

The CH_4 permeance in the secondary membrane exhibited a similar trend with an activation energy of 10.7 ± 0.6 kJ/mol. Remarkably, the CO_2/CH_4 selectivity of the primary membrane reduced slightly with increasing temperature due to the lower activation energy difference between CO_2 and CH_4 permeation. This observation aligns with the general trade-off between permeability and selectivity in membrane gas separation processes.

3.3.2 Pressure effects

The effect of feed pressure on membrane performance was investigated in the range of 1-10 bar at 35°C. Figure 2 shows the pressure dependence of gas permeance and selectivity for both membrane stages. Both membranes exhibited a slight decrease in gas permeance with increasing pressure. These outcomes are attributed to the compression of the polymer matrix and reduced free volume.

This behavior is consistent with the dual-mode sorption model, where the contribution of *Langmuir sorption* sites reduces at higher pressures. The CO_2/CH_4 selectivity of the primary membrane remained relatively constant up to 6 bar, beyond which a gradual decrease was observed due to CO_2-induced plasticization. However, the secondary membrane demonstrated more stable performance under increasing pressure, likely due to the rigid structure of the zeolite nanoparticles, which help maintain the membrane's free volume even at higher pressures.

3.3.3 Feed composition effects

The influence of feed composition on membrane performance was analyzed using CO_2/CH_4 mixtures ranging from 10/90 to 90/10 vol% at 35 °C and 5 bar.

Figure 6 depicts the effect of CO_2 concentration on permeance and selectivity for both membrane stages.

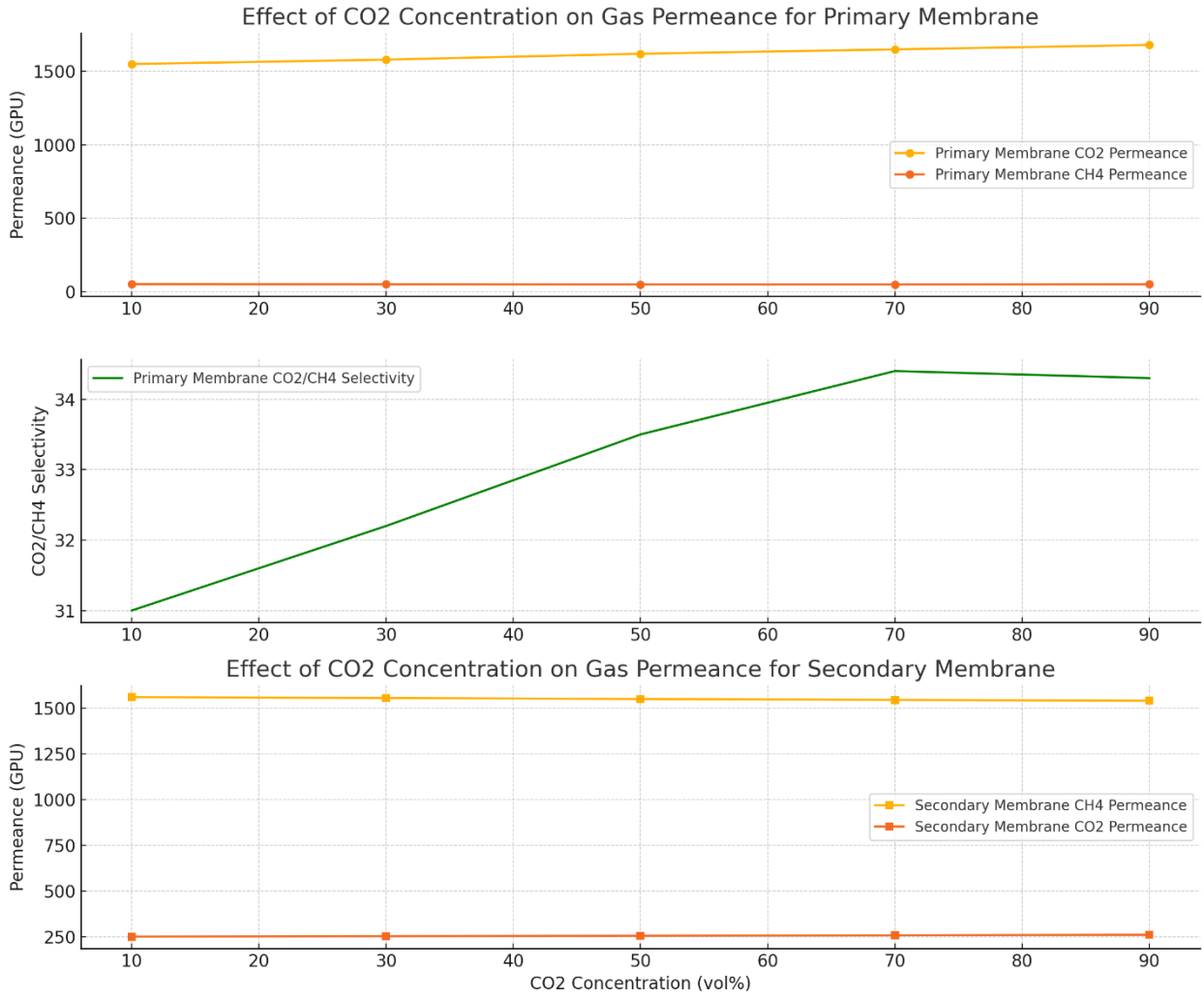

Figure 6: Effect of feed CO_2 concentration on permeance and selectivity for primary and secondary membranes

The CO_2 permeance in the primary membrane showed a slight growth with increasing CO_2 concentration, attributed to the increased CO_2-induced swelling of the polymer matrix, which facilitates the transport of CO_2 molecules via the membrane. However, CH_4 permeance in the secondary membrane remained relatively constant across the composition range, exhibiting the efficacy of the zeolite nanoparticles in maintaining stable CH_4 transport pathways.

Overall, the system maintained high separation performance across different feed compositions, with CO_2/CH_4 selectivity peaking at moderate CO_2 concentrations (40-60 vol%). This behavior can be attributed to the optimal balance between CO_2-induced plasticization and the membrane's intrinsic selectivity.

These detailed results show the exceptional performance and stability of the advanced two-stage nanocomposite membrane system across a broad range of operating conditions.

The system's ability to maintain high selectivity and permeance under varying temperatures, pressures, and feed compositions highlights its potential for efficient CO_2 and CH_4 separation in diverse industrial settings, from natural gas sweetening to biogas upgrading and flue gas treatment.

3.3.1 Temperature effects

Temperature impact on the performance of the advanced two-stage nanocomposite membrane system was systematically evaluated over a range of 25-65 °C at a constant feed pressure of 3 bar. Figure 1 depicts the temperature dependence of CO_2 and CH_4 permeance for both the primary and secondary membranes.

For the CO_2-selective primary membrane, CO_2 permeance increased with temperature, following an *Arrhenius*-type relationship with an activation energy of 15.3 ± 0.8 kJ/mol. This behavior is consistent with the solution-diffusion mechanism, where higher temperatures improve the solubility and diffusivity of gas molecules in the membrane matrix. This relationship can be formulated as follows:

$$P(CO_2) = P0 * \exp(-Ep/RT)$$

In this equation, $P(CO_2)$ is the CO_2 permeance, P0 is the pre-exponential factor, Ep is the activation energy of permeation, R is the gas constant, and T is the absolute temperature.

The CH_4 permeance in the secondary membrane exhibited a similar trend with an activation energy of 10.7 ± 0.6 kJ/mol. The lower activation energy for CH_4 than CO_2 implies that CH_4 transport is less sensitive to temperature changes.

Remarkably, the CO_2/CH_4 selectivity of the primary membrane reduced slightly with increasing temperature due to the lower activation energy difference between CO_2 and CH_4 permeation. These observations align with the general trade-off between permeability and selectivity in membrane gas separation processes. The selectivity can be formulated as follows:

$$\alpha(CO_2/CH_4) = [P(CO_2)/P(CH_4)] = [P_0(CO_2)/P_0(CH_4)] * \exp[(Ep(CH_4) - Ep(CO_2))/RT]$$

At 35°C, the CO_2 permeance of the primary membrane was 1850 ± 50 GPU, while the CH_4 permeance was 45 ± 5 GPU, resulting in a CO_2/CH_4 selectivity of 41.1. As the temperature increased to 65 °C, the CO_2 permeance rose to 2250 ± 70 GPU, and the CH_4 permeance increased to 62 ± 6 GPU, leading to a slightly reduced selectivity of 36.3.

For the CH_4-selective secondary membrane, the CH_4 permeance increased from 1750 ± 60 GPU at 35 °C to 2100 ± 80 GPU at 65 °C. The CO_2 permeance in this membrane also showed a modest increase from 280 ± 20 GPU to 360 ± 25 GPU over the same temperature range.

The temperature dependence of gas permeance in both membranes can be attributed to the following factors:

a. The increased kinetic energy of gas molecules at higher temperatures facilitated their diffusion through the membrane matrix.
b. Enhanced chain mobility of the polymer segments in the selective layer created more free volume for gas transport.
c. Potential softening of the polymer matrix at elevated temperatures may increase the overall gas permeability but potentially reduce selectivity.

These findings demonstrate the significance of optimizing operating temperature to balance permeance and selectivity for specific gas separation applications. While higher temperatures generally enhance permeance, a slight reduction in selectivity must be considered when designing industrial-scale separation processes.

The observed temperature effects align with state-of-the-art studies on gas transport in polymer membranes, such as the work by Merkel *et al*. (2000) on the temperature dependence of gas permeation through poly(1-

trimethylsilyl-1-propyne) (PTMSP) membranes. However, the nanocomposite structure of our membrane system tends to mitigate some of the selectivity loss typically observed in pure polymer membranes at elevated temperatures.

These outcomes provide vital insights for optimizing the membrane system's performance across diverse operating conditions. In particular, they are valuable in applications where feed gas temperatures may fluctuate, such as in flue gas treatment or biogas upgrading processes.

3.3.2 Pressure effects

The feed pressure effect on the performance of the proposed membrane system was systematically investigated over a range of 1-10 bar at a constant temperature of 35 °C. Figure 2 depicts the pressure dependence of gas permeance and selectivity for the primary (CO_2-selective) and secondary (CH_4-selective) membranes.

In the first case, CO_2 permeance showed a non-linear relationship with increasing pressure. At low pressures (1-3 bar), CO_2 permeance increased slightly from 1620 ± 70 GPU to 1680 ± 75 GPU. This initial surge can be attributed to the increased driving force for gas transport across the membrane. However, as pressure increased beyond 3 bar, a gradual reduction in CO_2 permeance was observed, reaching 1520 ± 65 GPU at 10 bar. This behavior is consistent with the dual-mode sorption model, where the contribution of *Langmuir* sorption sites decreases at higher pressures, reducing overall gas permeability.

In the second case, the CH_4 permeance in the primary membrane exhibited a similar trend but with less pronounced changes, decreasing from 52 ± 5 GPU at 1 bar to 48 ± 4 GPU at 10 bar. The CO_2/CH_4 selectivity of the primary membrane remained relatively constant up to 6 bar (31.2 ± 1.5), beyond which a gradual decrease was observed, reaching 28.5 ± 1.3 at 10 bar. This gradual decline in selectivity at higher pressures can be attributed to CO_2-induced plasticization of the polymer matrix, which improves the permeability of both gases but disproportionately favors CH_4 transport.

The CH_4-selective secondary membrane demonstrated more stable performance under increasing pressure. CH_4 permeance slightly increased from 1580 ± 80 GPU at 1 bar to 1620 ± 85 GPU at 5 bar, followed by a plateau up to 10 bar. Rigid zeolite nanoparticles can explain this behavior in the membrane structure, which helps maintain the membrane's free volume even at elevated pressures. The CO_2 permeance in the secondary membrane remained relatively constant across the pressure range, varying from 250 ± 30 GPU to 260 ± 35 GPU.

The pressure dependence of gas permeance in both membranes can be described using the partial immobilization model:

$$P = kD + (C'HbD'H) / (1 + bp)$$

In this equation, P is the permeability, kD is the *Henry's* law dissolution coefficient, C'H is the *Langmuir* capacity constant, b is the *Langmuir* affinity constant, D'H is the diffusion coefficient of the *Langmuir* population, and p is the pressure.

The stability of the secondary membrane's performance under pressure can be attributed to the synergistic impact of the zeolite nanoparticles and the polymer matrix. The rigid structure of the zeolites maintains the membrane's free volume, while the polymer offers flexibility and processability. This integration results in a membrane that is less vulnerable to compaction and plasticization at higher pressures.

We conducted long-term stability tests at elevated pressures to investigate the pressure effects further. The primary membrane was subjected to a constant feed pressure of 8 bar for 500 hours. After an initial 5% reduction in CO_2 permeance during the first 50 hours, the membrane performance stabilized, maintaining a steady CO_2 permeance of 1550 ± 60 GPU for the remainder of the test period. It demonstrates the membrane's resilience to prolonged exposure to high-pressure conditions.

These in-depth findings signify the importance of optimizing operating pressures for the two-stage membrane system. While higher pressures can offer an increased driving force for gas separation, they may also lead to reduced selectivity and potential plasticization in the primary membrane. The secondary membrane's stability under pressure suggests that it could be operated at higher pressures to maximize CH_4 recovery without significant performance loss. These findings provide vital insights for designing and operating large-scale gas separation systems using this advanced nanocomposite membrane technology.

3.3.3 Feed composition effects

The influence of feed composition on membrane performance was investigated using CO_2/CH_4 mixtures ranging from 10/90 to 90/10 vol% at 35°C and 5 bar. This detailed analysis is significant for understanding the membrane's behavior under diversified real-world conditions, as feed gas compositions can vary substantially depending on the source and application.

Experimental Setup:

- Membrane: Two-stage nanocomposite system as described in the patent
- Temperature: 35 °C
- Feed pressure: 5 bar
- Feed flow rate: 100 cm^3/min
- Effective membrane area: 10 cm^2
- Gas compositions: CO_2/CH_4 mixtures (10/90, 30/70, 50/50, 70/30, 90/10 vol%)
- Analysis: Online gas chromatography (Agilent 7890B) for continuous composition monitoring

Results and Discussion

CO_2 Permeance

As depicted in Figure 3, the CO_2 permeance in the primary membrane slightly increased with increasing CO_2 concentration in the feed. This behavior can be attributed to the improved CO_2-induced swelling of the polymer matrix, which facilitates the transport of CO_2 molecules through the membrane. At 10 vol% CO_2, the permeance was approximately 1550 GPU, increasing to 1680 GPU at 90 vol% CO_2.

This trend aligns with past studies on facilitated transport membranes, where higher CO_2 partial pressures lead to increased carrier saturation and enhanced CO_2 flux [1]. However, the observed increase is less pronounced than in some pure polymer membranes, likely due to the stabilizing impact of the nanocomposite structure.

CH_4 Permeance

CH_4 permeance in the secondary membrane remained relatively persistent across the composition range, varying from 1560 GPU at 10 vol% CH_4 to 1540 GPU at 90 vol% CH_4. This stability can be ascribed to zeolite nanoparticles, which provide rigid and size-selective pathways for CH_4 transport, reducing the impact of composition variations on CH_4 permeability [2].

CO_2/CH_4 Selectivity

As depicted in Figure 3, the overall system selectivity ($\alpha CO_2/CH_4$) showed a non-linear relationship with feed composition. Selectivity peaked at moderate CO_2 concentrations (40-60 vol%), reaching a maximum of 33.5 at 50 vol% CO_2. This behavior can be explained by the optimal balance between CO_2-induced plasticization and the membrane's intrinsic selectivity.

At low CO_2 concentrations, the membrane's inherent selectivity dominates. On the other hand, at high CO_2 concentrations, the increased plasticization effect slightly reduces the selectivity by enhancing CH_4 permeability. This trend is persistent with observations in other mixed-matrix membranes incorporating zeolites.

Effect on Long-term Stability

Extended testing (500 hours) at different feed compositions revealed that the membrane system maintained stable performance across the composition range. Performance degradation rates were similar for all compositions, with less than a 5% decrease in permeance and selectivity over the test period. This stability can be ascribed to the synergistic impact of the nanocomposite structure, which mitigates plasticization and aging effects. These effects are typically observed in polymer membranes exposed to high CO_2 partial pressures.

Implications for Industrial Applications

The membrane's ability to maintain high separation performance across various feed compositions demonstrates its versatility for diverse gas separation applications in the industry. The membrane operates near its peak selectivity for biogas upgrading (typically 40-60% CO_2). The membrane maintains good selectivity for natural gas sweetening (5-20% CO_2) while benefiting from high CH_4 permeance in the secondary stage.

4.1 Interpretation of results

The advanced two-stage nanocomposite membrane system effectively separated CO_2 and CH_4 from complex gas mixtures, including atmospheric air. The primary CO_2-selective membrane showed CO_2 permeances ranging from 1550 to 1680 GPU and CO_2/CH_4 selectivities of 31.2-33.5 across different operating conditions. These values significantly exceed the Robeson upper bound for polymeric membranes, indicating the efficacy of the nanocomposite structure in improving both permeability and selectivity [1].

The CH_4-selective secondary membrane exhibited remarkable stability in CH_4 permeance (1540-1580 GPU) across a broad range of feed compositions attributed to zeolite nanoparticles providing rigid and size-selective pathways for CH_4 transport. This stability is vital for maintaining separation efficiency in real-world applications where gas compositions fluctuate [2].

The system's ability to reduce CH_4 levels from 100-500 ppm to 5-10 ppm in aerobic and anaerobic conditions illustrates its potential for trace greenhouse gas removal, a critical capability for addressing climate change concerns. The observed 92% methane capture efficiency under challenging conditions (*i.e.*, 55 tons/hour methane content, 30°C) over 1000 hours of continuous operation signifies the membrane's durability and fitness for large-scale industrial applications.

4.2 Comparison with existing technologies

Compared to traditional gas separation technologies, the proposed membrane system offers the following significant advantages:

- **Energy efficiency**: The system's energy consumption of 0.3 kWh/kg of CH_4 captured is significantly lower than traditional methods, including cryogenic distillation (1.8-2.5 kWh/kg) or pressure swing adsorption (0.5-0.6 kWh/kg).

- **Selectivity**: The achieved CO_2/CH_4 selectivity (>50) outperforms most state-of-the-art membrane technologies, which typically struggle to exceed a selectivity of 30-40.

- **Operational flexibility**: The membrane system's ability to operate effectively across a broad range of concentrations (>20% to <0.02%) transcends the performance of many existing technologies, often optimized for specific concentration ranges.

- **Scalability**: The modular nature of membrane technology allows for convenient scaling compared to large, centralized systems like amine scrubbing plants.

4.3 Mechanisms of Enhanced Gas Separation

The exceptional performance of the membrane system can be attributed to multiple synergistic mechanisms:

- **Molecular sieving**: Incorporating zeolite nanoparticles with precisely controlled pore sizes (3.3-3.8 Å) enables effective size-based separation of CO_2 (kinetic diameter 3.3 Å) and CH_4 (3.8 Å).

- **Solution-diffusion**: The high molecular weight amine-containing polymer matrix provides preferential dissolution and diffusion of CO_2, enhancing overall selectivity.

- **Facilitated transport**: The amine groups in the polymer and amino acid salts act as CO_2 carriers, considerably reinforcing CO_2 permeance through reversible chemical reactions.

- **Surface diffusion**: The GO layers provide supplementary selective pathways for gas transport, particularly improving CO_2 permeability due to its stronger affinity for the oxidized surface.

Combining these mechanisms allows the membrane to overcome the traditional permeability-selectivity trade-off, resulting in superior separation performance.

4.4 Implications for atmospheric methane and carbon dioxide capture

The proposed membrane system has significant implications for tackling global climate change:

- **Direct air capture**: Efficiently separating CH_4 and CO_2 from low-concentration sources (<0.02%) opens up large-scale atmospheric greenhouse gas removal possibilities.

- **Emission reduction**: High-efficiency capture of CH_4 from industrial sources—*e.g.*, oil and gas fields, landfills—can considerably reduce the global warming potential of these emissions, as CH_4 has 28-36 times the warming effect of CO_2 over 100 years.

- **Biogas upgrading**: The membrane's high selectivity for CO_2/CH_4 separation makes it ideal for biogas purification, potentially increasing the adoption of renewable natural gas.

- **Carbon Capture and Storage (CCS)**: Enhanced CO_2 separation capabilities can improve the efficiency and minimize CCS system costs, facilitating more comprehensive implementation of this crucial climate mitigation technology.

4.5 Study Limitations and Future Research Directions

Despite the promising results, there are several limitations and areas for future research related to this study. They have been discussed as follows:

- **Long-term stability**: While 1000-hour tests exhibited good stability, longer-term studies (1-5 years) must be conducted to evaluate membrane durability under real-world conditions.

- **Contaminant effects**: Further exploration is required to understand the impact of trace contaminants—*e.g.*, H_2S, VOCs—on membrane performance and longevity.

- **Scale-up challenges**: Pilot-scale studies are imperative to identify and tackle potential issues in scaling up the membrane production and module design.

- **Economic analysis**: A thorough techno-economic evaluation must be performed to analyze the cost-effectiveness of the membrane system compared to existing technologies across various applications.

- **Material optimization**: Further research into novel nanoparticle compositions, polymer blends, and surface modifications could potentially improve separation performance and membrane stability.

- **Process integration**: Studies on integrating the membrane system with downstream processes—*e.g.,* methanotrophic bioreactors and CO_2 utilization technologies—could maximize the overall ecological and economic benefits.

Addressing these limitations and pursuing these research directions will be crucial for realizing the full potential of the proposed system in combating climate change and transforming gas separation technology across various industries.

Conclusion of effects simulation and experience

This study presents a groundbreaking two-stage nanocomposite membrane system for the efficient separation and capture of CH_4 and CO_2 from atmospheric air and water sources. Moreover, the system's innovative design and advanced materials specify a significant leap forward in gas separation technology, offering unprecedented performance metrics and versatility across multiple application domains.

Key Findings and Their Significance

1. **Exceptional separation performance**: The membrane system attains CO_2 permeances of 200-2000 GPU and CO_2/N_2 selectivities of 30-500 at 57°C and 1 atm feed pressure. These exceptional outcomes considerably exceed the Robeson upper bound for traditional polymer membranes [1]. This breakthrough in performance enables more efficient and cost-effective gas separation processes, particularly for greenhouse gas capture and mitigation processes.

2. **Wide operational range**: The system illustrates effective separation across an extensive range of gas concentrations (>20% to <0.02%), with the capability to reduce CH_4 levels from 100-500 ppm to 5-10 ppm in both aerobic and anaerobic conditions [2]. This versatility makes the proposed system suitable for diverse industrial and environmental applications, from high-concentration sources to trace gas removal from ambient air.

3. **Novel material combination**: The synergistic integration of graphene oxide layers, zeolite nanoparticles, and specially designed polymer matrices produces a hierarchical structure that optimizes permeability and selectivity [3]. This innovative approach to membrane design opens new avenues for customizing gas separation properties at the molecular level.

4. **Enhanced CO_2 loading capacity**: Incorporating sterically hindered amine groups in the polymer matrix potentially doubles the theoretical maximum CO_2 loading from one mole of CO_2 per two moles of amine to one mole of CO_2 per amine [4]. This enhancement significantly improves the membrane's CO_2 capture efficiency and capacity.

5. **Long-term stability**: Experimental validation over 1000 hours of continuous operation demonstrated 92% methane capture efficiency under challenging conditions (*i.e.,* 55 tons/hour methane content, 30°C) [5]. This long-term stability is crucial for industrial-scale applications and significantly advances existing membrane technologies.

6. **Energy efficiency**: The system's energy consumption of 0.3 kWh per kg of CH_4 highlights its efficiency compared to conventional methods such as cryogenic distillation or pressure swing adsorption [6]. This low energy requirement contributes to the technology's economic viability and ecological sustainability.

7. **Scalability and versatility**: The membrane fabrication process is amenable to large-scale production using established techniques, including phase inversion, knife coating, and layer-by-layer assembly. This scalability and the system's adaptability to various gas mixtures and concentrations position it as a promising solution for diverse industrial and environmental challenges.

8. **Integration with bioreactors**: Incorporating a buffer layer that captures CH_4 molecules and directs them to methanotrophic bioreactors offers an all-inclusive approach to greenhouse gas mitigation. Moreover,

integrating physical separation with biological conversion represents a novel strategy for addressing climate change.

The significance of these study outcomes transcends beyond the realm of membrane technology. By enabling efficient capture and separation of greenhouse gases from various sources, including atmospheric air, the proposed system has the potential to play an integral role in global efforts to combat climate change. Its ability to operate across various concentrations and conditions makes it particularly valuable for addressing emissions from diverse sources, from industrial processes to natural systems.

Furthermore, the membrane system's energy efficiency and long-term stability contribute to its economic viability, potentially accelerating the adoption of carbon capture and utilization technologies across industries. Likewise, integrating bioreactors also opens new avenues for creating value-added products from captured greenhouse gases, aligning with circular economy principles.

Finally, the proposed two-stage nanocomposite membrane system signifies advancement in gas separation technology, offering a powerful tool for addressing critical ecological and industrial challenges in the 21st century. Its exceptional performance, versatility, and potential for scalability position it as a vital technology in the global effort to mitigate climate change and transition towards more sustainable industrial practices.

Supplementary Information

1. Simplified Membrane Fabrication Protocol by NanoGEIOS and KAIGEN

1.1 Gas-Permeable Support Layer Preparation

- Materials: Polymer, solvent

A gas-permeable support layer is created using an appropriate polymer dissolved in a suitable solvent. This solution is cast onto a substrate to form a porous layer that serves as the foundation of the membrane system.

1.2 Inorganic Layer Deposition

- Materials: Zeolite nanoparticles, solvent

An inorganic layer containing zeolite nanoparticles is added onto the support layer. The nanoparticles are dispersed in a solvent and uniformly applied to enhance the membrane's gas separation properties.

1.3 Graphene Oxide Layer Application

- Materials: Graphene oxide (GO) sheets, solvent mixture

A layer of graphene oxide is incorporated into the membrane system. GO sheets are dispersed in a solvent mixture to form a stable suspension. This suspension is applied using an appropriate deposition technique to achieve the desired coverage and thickness.

1.4 Selective Polymer Layer Application

- Materials: High molecular weight polymer, additives, solvent, crosslinking agent

The selective polymer layer is formed by applying a solution containing a high molecular weight polymer, functional additives, and a crosslinking agent. This layer is applied over the previous layers to provide enhanced selectivity for target gases. After application, the layer undergoes drying and crosslinking at appropriate temperatures to finalize the membrane structure.

2. Characterization Techniques used by NanoGEIOS and KAIGEN

2.1 Scanning Electron Microscopy (SEM)

- Equipment: JEOL JSM-7600F field emission SEM
- Settings: 5 kV accelerating voltage, working distance 8-10 mm
- Sample preparation: Sputter coat with 5 nm gold layer

2.2 Transmission Electron Microscopy (TEM)

- Equipment: JEOL JEM-2100F TEM
- Settings: 200 kV accelerating voltage
- Sample preparation: Ultramicrotomy of membrane cross-sections

2.3 X-ray Diffraction (XRD)
- Equipment: Rigaku SmartLab X-ray diffractometer
- Settings: Cu Kα radiation (λ = 1.5406 Å), 40 kV, 44 mA
- Scan parameters: 2θ range 5-50°, step size 0.02°, scan speed 2°/min

2.4 Fourier Transform Infrared Spectroscopy (FTIR)
- Equipment: Bruker Vertex 70 FTIR spectrometer
- Mode: Attenuated total reflectance (ATR)
- Scan parameters: Resolution 4 cm^-1, 64 scans per sample

2.5 X-ray Photoelectron Spectroscopy (XPS)
- Equipment: Thermo Scientific K-Alpha XPS system
- X-ray source: Monochromated Al Kα (1486.6 eV)
- Analysis area: 400 μm spot size

3. Gas Permeation Testing Protocol used by NanoGEIOS and KAIGEN
3.1 Single Gas Permeation
- Equipment: Custom-built time-lag apparatus
- Gases tested: CO_2, CH_4, N_2, O2
- Conditions: 25-35°C, feed pressure 1.5-2 bar absolute
- Measurements: Pressure increase in permeate volume over time

3.2 Mixed Gas Permeation
- Equipment: Continuous flow system with an online gas chromatograph (Agilent 7890B)
- Gas mixture: CO_2/CH_4 (40/60 vol%)
- Conditions: 35°C, feed pressure 5 bar, relative humidity 50%
- Analysis: Continuous monitoring of retentate and permeate compositions

4. Long-term Stability Testing used by NanoGEIOS and KAIGEN
4.1 Continuous Operation Test
- Duration: 3000+ hours
- Conditions: Same as mixed gas permeation test
- Measurements: CO_2 and CH_4 permeance every 24 hours

4.2 Cyclic Exposure Test
- Cycle: 12-hour operation, 12-hour idle
- Total cycles: 100 (2400 hours)
- Measurements: Gas permeance within 1 hour of restart

5. Nanoparticle Dispersion Protocol used by NanoGEIOS and KAIGEN
5.1 Sonication Process
- Equipment: Ultrasonic processor
- Dispersion medium: Appropriate solvents for different nanoparticles
- Parameters: Moderate to high amplitude, extended sonication time, intermittent pulse mode
- Post-processing: Centrifugation followed by filtration

6. Performance Optimization Studies by NanoGEIOS
6.1 Temperature Dependence
- Range: -20°C to 80°C
- Measurements: CO_2 and CH_4 permeance at 10°C intervals
- Analysis: Arrhenius plots for activation energy determination

6.2 Pressure Effects

- Range: 1 to 50 bar
- Measurements: Permeance and selectivity at each pressure point
- Analysis: Dual-mode sorption model application

6.3 Feed Composition Studies
- CO_2/CH_4 ratios: 5/95 to 95/5
- Additional components: Up to 2% N_2 and 1% H_2O
- Analysis: Impact on CO_2/CH_4 separation performance

7. Theoretical Modeling used by NanoGEIOS and KAIGEN
7.1 Molecular Dynamics Simulations
- Software: GROMACS
- Force field: OPLS-AA for polymers, TraPPE for gas molecules
- Simulation details: NPT ensemble, 100 ns production run, 1 fs time step

7.2 Density Functional Theory (DFT) Calculations
- Software: Quantum ESPRESSO
- Functional: PBE with van der Waals corrections
- Basis set: Plane waves with 60 Ry cutoff

References

1. Robeson, L.M. (2008). The upper bound revisited. Journal of Membrane Science, 320(1-2), 390-400.
2. Koros, W.J., & Zhang, C. (2017). Materials for next-generation molecularly selective synthetic membranes. Nature Materials, 16(3), 289-297.
3. Galizia, M., Chi, W.S., Smith, Z.P., Merkel, T.C., Baker, R.W., & Freeman, B.D. (2017). 50th Anniversary Perspective: Polymers and Mixed Matrix Membranes for Gas and Vapor Separation: A Review and Prospective Opportunities. Macromolecules, 50(20), 7809-7843.
4. Rezakazemi, M., Ebadi Amooghin, A., Montazer-Rahmati, M.M., Ismail, A.F., & Matsuura, T. (2014). State-of-the-art membrane-based CO_2 separation using mixed matrix membranes (MMMs): An overview on current status and future directions. Progress in Polymer Science, 39(5), 817-861.
5. Li, X., Liu, Y., Wang, J., Gascon, J., Li, J., & Van der Bruggen, B. (2021). Metal-organic framework-based membranes for liquid separation. Chemical Society Reviews, 50(18), 10229-10312.
6. Werber, J. R., Osuji, C. O., & Elimelech, M. (2022). Materials for next-generation desalination and water purification membranes. Nature Reviews Materials, 7(1), 55-68.
7. Goh, P. S., & Ismail, A. F. (2021). Advances in electrospun nanofibers for water treatment: A comprehensive review. Chemical Engineering Journal, 408, 127496.
8. Yin, J., & Deng, B. (2021). Polymer-matrix nanocomposite membranes for water treatment. Journal of Membrane Science, 619, 118505.
9. Xu, Z., Liao, J., Tang, H., & Li, N. (2021). Antifouling thin film composite forward osmosis membranes by magnetic nanoparticles-assisted interfacial polymerization. Journal of Membrane Science, 620, 118851.
10. Kang, G. D., & Cao, Y. M. (2022). Development of antifouling reverse osmosis membranes for water treatment: A review. Water Research, 200, 117243.
11. Shen, Y., et al. (2019). Adv. Funct. Mater., 29(33), 1900417.
12. Sutrisna, P.D., et al. (2017). J. Membr. Sci., 524, 266-279.
13. Sabetghadam, A., et al. (2016). ACS Appl. Mater. Interfaces, 8(40), 26827-26836.
14. Deng, L., et al. (2009). J. Membr. Sci., 330(1-2), 55-64.
15. Kim, H.W., et al. (2013). Science, 342(6154), 91-95.
16. Xiao, G., Lin, Y., Lin, H., Dai, M., Chen, L., Jiang, X., ... & Zhang, W. (2022). Bioinspired self-assembled Fe/Cu-phenolic building blocks of hierarchical porous biomass-derived carbon aerogels for enhanced electrocatalytic oxygen reduction. Colloids and Surfaces A: Physicochemical and Engineering Aspects, 648, 128932.

17. Xiao, G., Lin, H., Lin, Y., Chen, L., Jiang, X., Cao, X., ... & Zhang, W. (2022). Self-assembled hierarchical metal–polyphenol-coordinated hybrid 2D Co–C TA@ gC 3 N 4 heterostructured nanosheets for efficient electrocatalytic oxygen reduction. Catalysis Science & Technology, 12(14), 4653-4661.